

Supporting Information

Zn(II)-Functionalized COF as a Recyclable Catalyst for the Sustainable Synthesis of Cyclic Carbonates and Cyclic Carbamates from Atmospheric CO₂

Somnath Sarkar^{a,‡}, Swarbhanu Ghosh^{a,b,‡}, Sk. Manirul Islam^{a,*}

^aDepartment of Chemistry, University of Kalyani, Kalyani, Nadia, West Bengal-741235 (India).

^bDepartment of Chemistry, Indian Institute of Technology (IIT) Madras, Chennai 600036, India

[‡]Authors contributed equally

*E-mail:manir65@rediffmail.com

Materials and Equipments

Some unsaturated amines (i.e., 3a, 3b, 3d, 3e and 3f) and all epoxides were purchased from a commercial supplier. ¹H NMR spectra were recorded on Bruker DPX-300/500 NMR spectrometer. NMR spectra were recorded at 298 K.

A D8 Advance SWAX diffractometer from Bruker-AXS utilizing a constant current (40 mA) and voltage (40 kV) was used to obtain the powder XRD pattern of the Zn(II) decorated COF catalyst. The XRD machine was calibrated with silicon sample utilizing Ni-filtered Cu K α radiation ($\lambda=0.15406$ nm). Quantachrome Autosorb-iQ (USA) surface area analyser was used for N₂ adsorption/desorption analysis at 77 K. The sample was activated at 403 K for 12 h under high vacuum before the adsorption of gas. Pore size distribution was obtained by using NLDFT method employing the carbon/cylindrical pore model as reference. For the analysis of HR TEM, 10 mg of the Zn@TpTta catalyst was dispersed into absolute EtOH under the application of sonication for 5 min, followed by the sample coating on a carbon coated Cu-grid and dried in air. JEOL JEM 6700 field emission-scanning electron microscope (FE SEM) was employed to analyze particle size and morphology of Zn@TpTta. UV-visible diffuse reflectance spectroscopy (UV 2401PC) and FT-IR (Nicolet MAGNA-FT IR 750 spectrometer Series II) were used to understand the framework and coordination. A TA Instruments thermal analyser (TA-SDT Q-600) was used for thermogravimetric (TGA) of Zn(II) decorated COF with a temperature (ramped at 10°C/min) under continuous air flow. A CHNOS elemental analyser (Vario EL III) was used to determine the contents of C, N and H

in Zn@TpTta. ^1H spectra of the desired products were kept on a Bruker DPX-300/500 NMR spectrometer.

Computational Study:

All the computational simulations were carried out using the Gaussian 16 program with a meta-hybrid GGA functional M06. We have used a mixed basis set 6-31G(d) for H, C, N, O, and Cl, whereas the heavier atoms Zn and Br were treated with a “double- ξ ” quality basis set consisting of effective core potentials (LanL2DZ ECP). The method and theories adopted in this study were successfully applied to similar thermochemical investigations. The geometry optimization was followed by vibrational frequency analysis and all the reactants, intermediates (Int), and products were confirmed with no imaginary frequencies. Whereas the transition states (TS) were confirmed with only one imaginary frequency.

Kinetic curves for the generation of cyclic carbamate:

We have studied the conversion rates with time for the production of cyclic carbamate in presence of Zn@TpTta catalyst and from the collected data, the kinetic curves (Figure S1) have been plotted. We have also performed a comparative study of the conversion rates among several recycling runs for the generation of the cyclic carbamate (Figure S2). This figure elicits that after five successive runs there was an inconsiderable change in the conversion rates which indicates that the reusability of the Zn@TpTta catalyst is extremely high, retaining its initial activity.

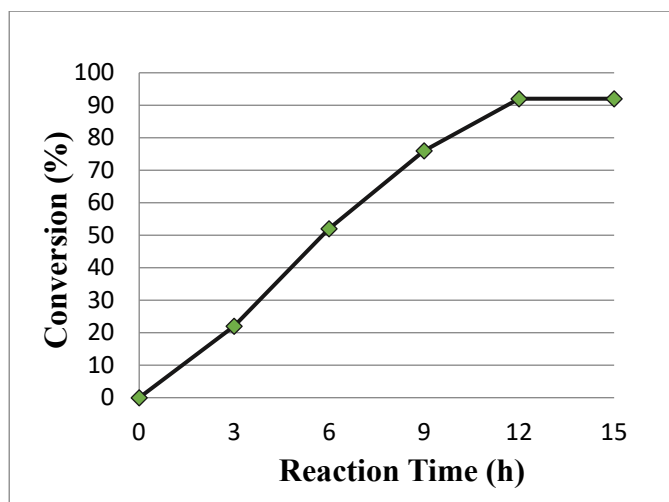


Figure S1. Kinetic curve for generation of the cyclic carbamate (the atmospheric cyclization of **3a**).

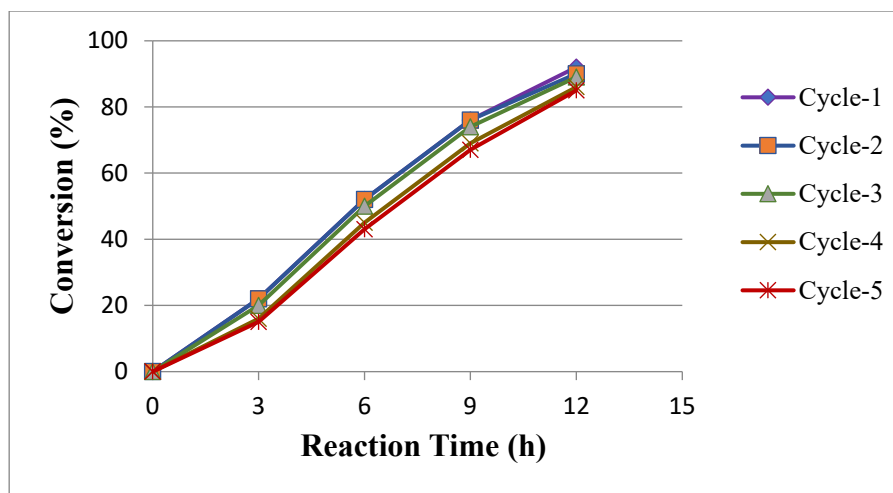


Figure S2. Comparison study of conversion rates among several recycling runs for the generation of the cyclic carbamate (the atmospheric cyclization of **3a**).

FTIR spectra:

Formation of TFP from phloroglucinol was analyzed by FTIR analysis technique as shown in Fig S3. The absorption occurred around 3472, 3340 and 3197 cm^{-1} correspond to O-H stretching vibration and a strong peak at 1616 cm^{-1} corresponds to C=C stretching vibration present in the phloroglucinol moiety. Along with these characteristic stretching frequencies for phloroglucinol, two new peaks appeared at 1643 and 2889 cm^{-1} indicating the presence of C=O and aliphatic C-H stretching frequencies corresponding to the aldehyde group which confirms the formation of triformylphloroglucinol (TFP).¹ On the other hand, the peak appeared at around 3478, 3372 and 3212 cm^{-1} indicate stretching mode and the peak at 1626 cm^{-1} indicate the bending mode of the primary amine (N-H) group along with the characteristic peak of C≡N (2215 cm^{-1}) present in the 4-aminobenzonitrile moiety.² But in the case of TAPT moiety, the absence of characteristic C≡N (2215 cm^{-1}) stretching frequency and the appearance of C=N stretching frequency at 1633 cm^{-1} confirms the successful formation of TAPT, keeping the characteristics N-H and C=C stretching frequencies almost constant (Fig. S4).³

Comparison of FTIR spectra of the reactants (TP and Tta) with TpTta and Zn@TpTta has been exhibited in Fig. S5. The IR spectra of TpTta clearly shows that the COF (TpTta) was obtained by total consumption of both the starting materials as there is an absence of characteristics stretching vibration of N-H modes (3462, 3323, 3212 cm^{-1}) of primary amine of TAPT and C=O stretching frequency (1643 cm^{-1}) as well as aliphatic C-H stretching frequency (2889 cm^{-1}) of TFP.³ The presence of the N-H stretching vibration mode of secondary amine at 3410 cm^{-1} and 3434 cm^{-1} of TpTta and Zn@TpTta respectively clearly

confirmed that the obtained solid product exists mainly in β -ketoenamine form arising due to the tautomerism between hydroxyl (-OH) units at β -positioned and Schiff bonds (-C=N-). In case of β -ketoenamine form, there is loss of aromaticity of the benzene ring of TFP, so it seems that this form is a little bit unstable compare to its enol form, but actually, the loss of aromaticity was accompanied by stabilization arising from the higher basicity of nitrogen over phenolic oxygen which led to extremely thermal as well as chemical stability.⁴

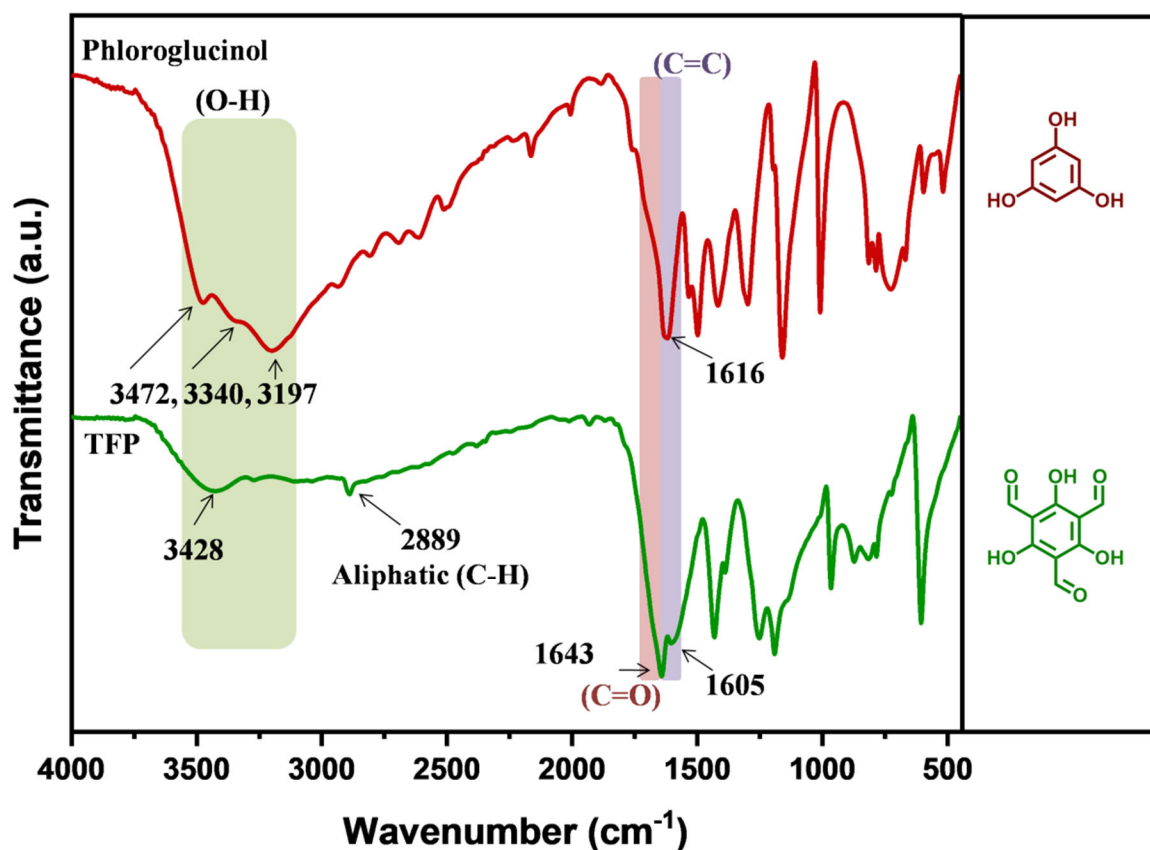


Figure S3. FTIR spectra of phloroglucinol and TFP.

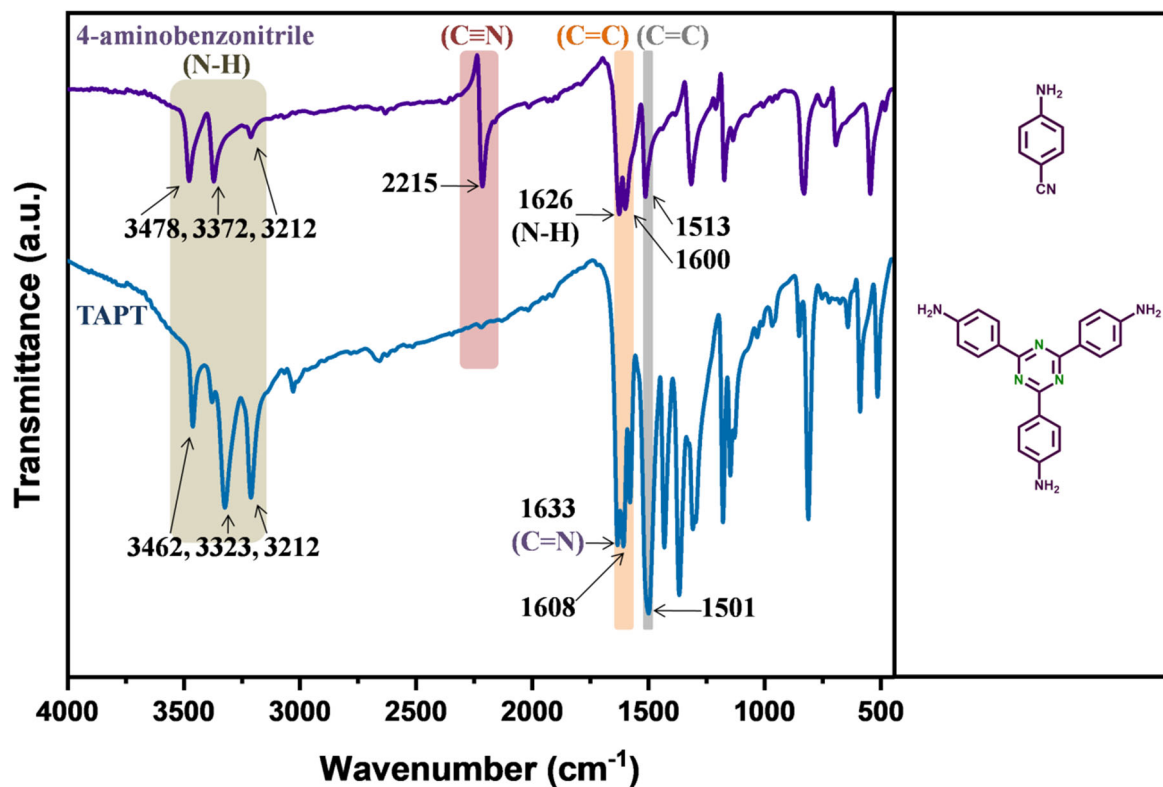


Figure S4. FTIR spectra of 4-aminobenzonitrile and TAPT.

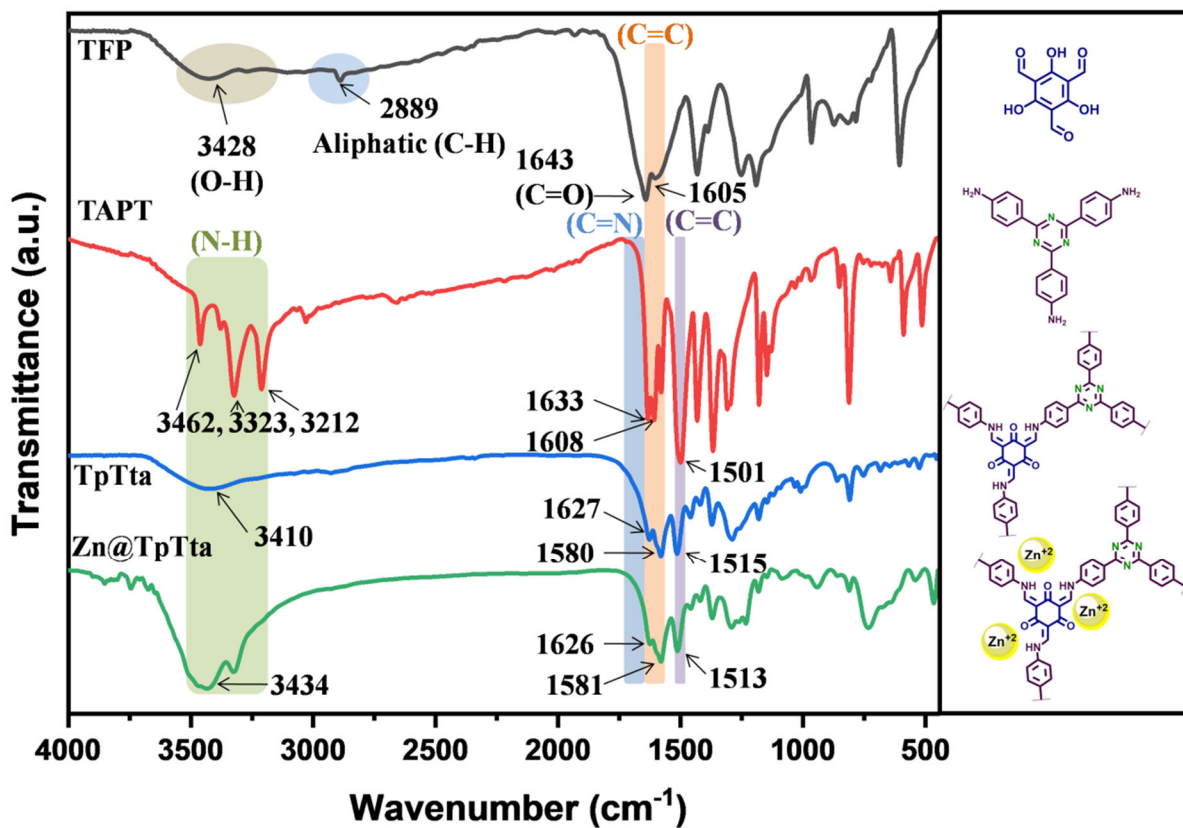
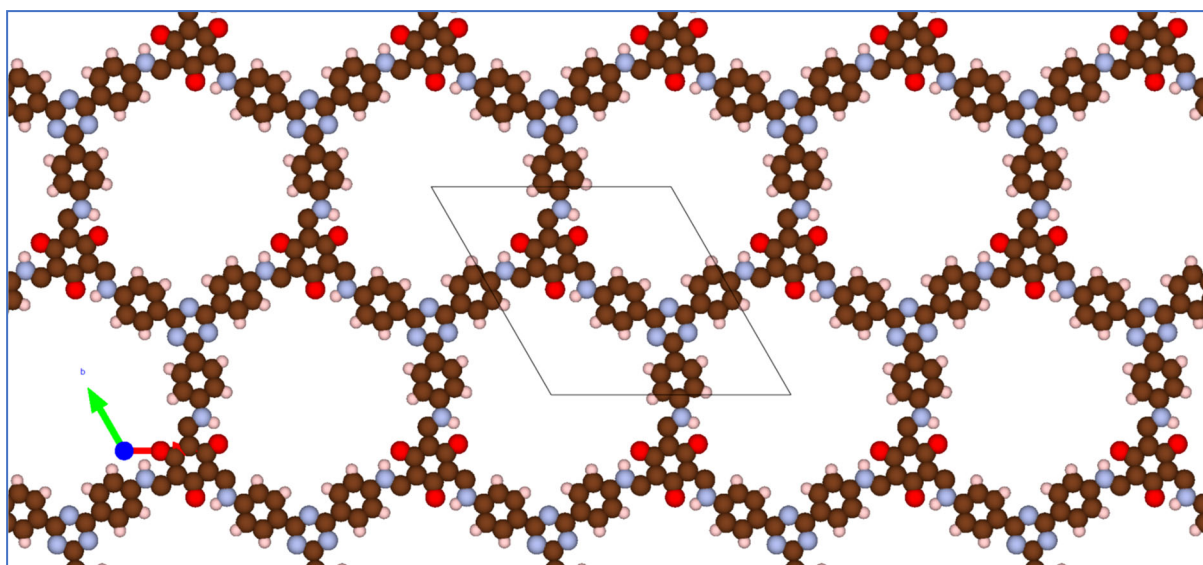


Figure S5. FTIR spectra of TFP, TAPT, TpTta and Zn@TpTta.

AA stacking arrangement of TpTta (eclipsed structure):



Lattice type: P
Space group name: P -6
Space group number: 174
Setting number: 1

Lattice parameters

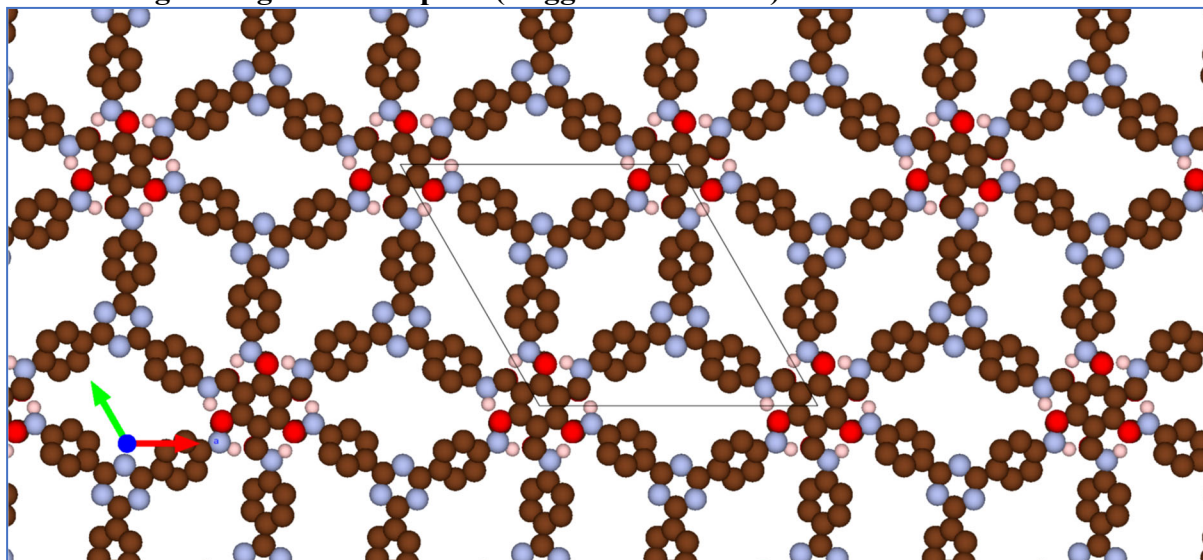
a **b** **c** **alpha** **beta** **gamma**
18.15900 **18.15900** **3.49700** **90.0000** **90.0000** **120.0000**

Structure parameters:

			x	y	z	Occ.	U	Site
Sym.								
1	H	H1	0.13431	0.66018	0.49265	1.000	0.000	6l
2	C	C2	0.15464	0.56364	3.50000	1.000	0.000	3k
3	N	N3	0.10738	0.59749	3.50000	1.000	0.000	3k
4	C	C4	-0.15691	0.43862	3.50000	1.000	0.000	3k
5	C	C5	-0.10235	0.40528	3.50000	1.000	0.000	3k
6	H	H6	-0.12561	0.34534	3.50000	1.000	0.000	3k
7	C	C7	-0.01667	0.45691	3.50000	1.000	0.000	3k
8	H	H8	0.01947	0.43286	3.50000	1.000	0.000	3k
9	C	C9	0.01824	0.54298	3.50000	1.000	0.000	3k
10	C	C10	-0.03574	0.57862	3.50000	1.000	0.000	3k
11	H	H11	-0.01218	0.63874	3.50000	1.000	0.000	3k
12	C	C12	-0.12258	0.52527	3.50000	1.000	0.000	3k
13	H	H13	-0.15920	0.54868	3.50000	1.000	0.000	3k
14	C	C14	0.36741	0.75401	0.50000	1.000	0.000	3
15	C	C15	0.28036	0.70135	0.50000	1.000	0.000	3k
16	O	O16	0.23669	0.72988	0.50000	1.000	0.000	3k
17	C	C17	0.61655	0.36657	0.50000	1.000	0.000	3k
18	N	N18	0.70015	0.41959	0.50000	1.000	0.000	3k

Number of polygons and unique vertices on isosurface = 0 (0)
 4599 atoms, 5535 bonds, 0 polyhedra; CPU time = 96 ms

AB stacking arrangement of TpTta (staggered structure):



Lattice type: P
Space group name: P-3
Space group number: 147
Setting number: 1

Lattice parameters:

a **b** **c** **alpha** **beta** **gamma**
18.38920 **18.38920** **9.19190** **90.0000** **90.0000** **120.0000**

Structure parameters

			x	y	z	Occ.	U	Site
Sym.								
1	C	C1	0.42072	0.70086	0.31068	1.000	0.000	6g
2	N	C2	0.38620	0.75355	0.31023	1.000	0.000	6g
3	C	C3	0.51200	0.73695	0.30146	1.000	0.000	6g
4	C	C4	0.54570	0.69631	0.22415	1.000	0.000	6g
5	C	C5	0.63216	0.73276	0.20607	1.000	0.000	6g
6	C	C6	0.68664	0.81253	0.26488	1.000	0.000	6g
7	C	C7	0.65257	0.85164	0.35090	1.000	0.000	6g
8	C	C8	0.56574	0.81360	0.36571	1.000	0.000	6g
9	N	N9	0.77486	0.84969	0.23984	1.000	0.000	6g
10	C	C10	0.82258	0.92820	0.21005	1.000	0.000	6g
11	C	C11	0.91274	0.96393	0.19300	1.000	0.000	6g
12	C	C12	0.94903	0.91282	0.19358	1.000	0.000	6g
13	O	O	0.82789	0.93610	0.81291	1.000	0.000	6g
14	H	H	0.81308	0.82037	0.21135	1.000	0.000	6g

=====

=

Number of polygons and unique vertices on isosurface = 0 (0)
 6764 atoms, 8116 bonds, 0 polyhedra; CPU time = 69 ms

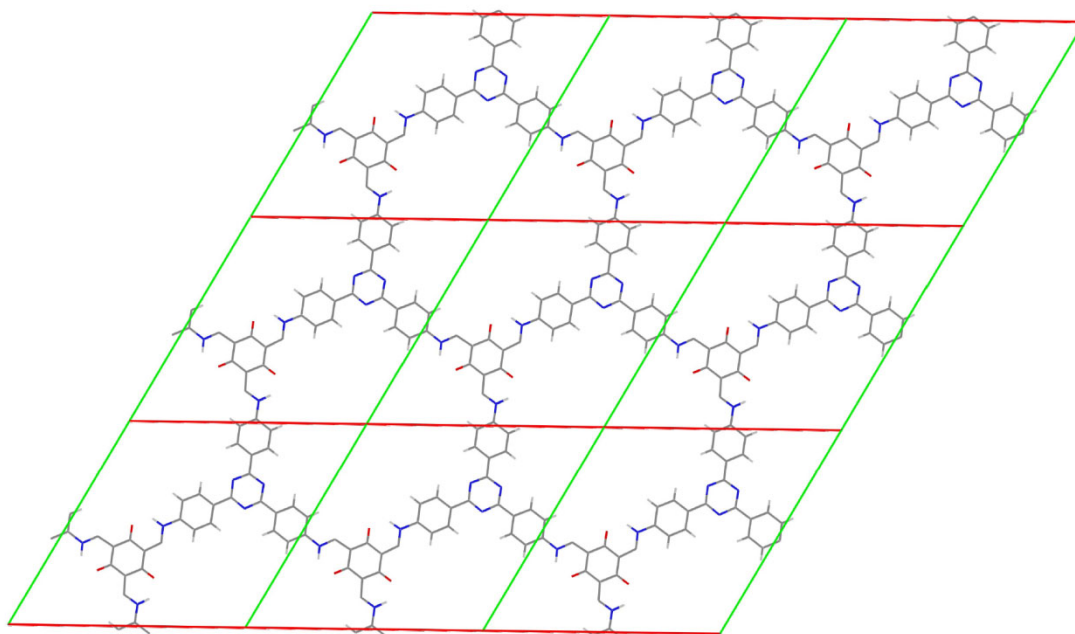


Figure S6. 3×3 unit cell of AA stacked COF.

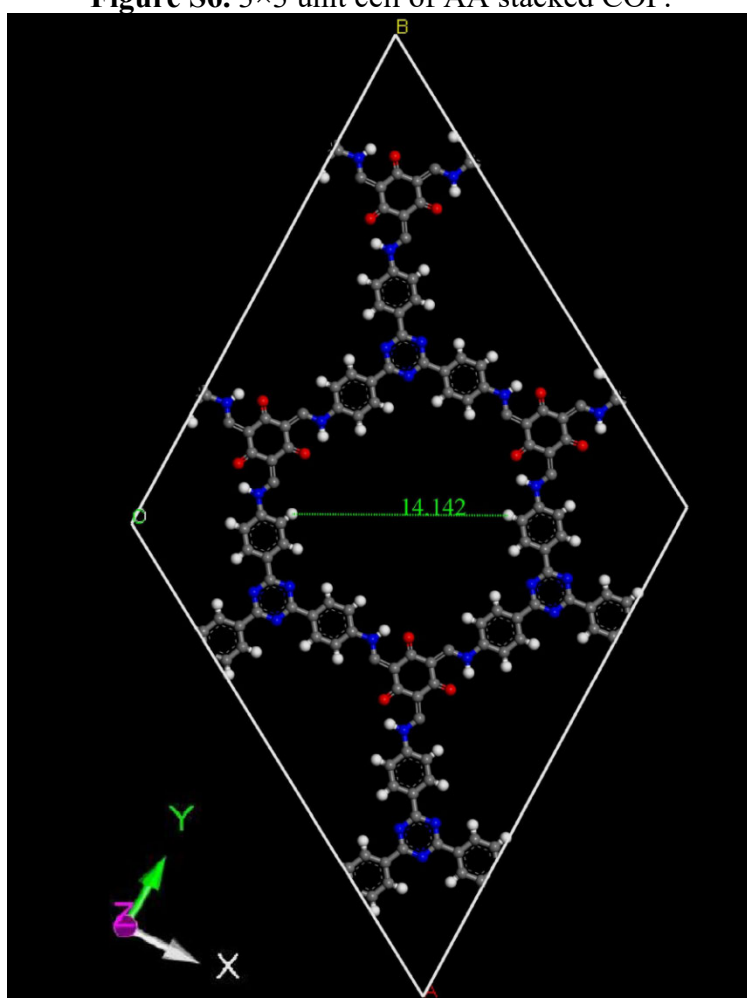
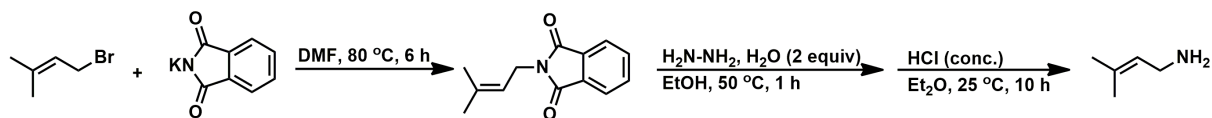


Figure S7. 2×2 unit cell of AA stacked COF (TpTta), displaying pore size of about 1.41 nm.

1. Experimental Section

Typical methods for the synthesis of unsaturated amine derivatives

Method for the synthesis of unsaturated amine 1c:



A solution of prenyl bromide (30 mmol) and potassium phthalimide (30 mmol) in a suitable solvent (DMF) was allowed to stir for 6 h at a definite temperature (80 °C) under N₂ atmosphere. Then the mixture was allowed to cool to room temperature. After that, the resultant solution was poured into an ice-water system and the solid was carefully collected on a filter funnel. The obtained crude product was used with no further purification. Hydrazine monohydrate (60 mmol) was allowed to pour into a solution of *N*-prenylphthalimide and ethanol (250 mL) at 50 °C. The reaction mixture was subjected to stir for a particular time (1 h) and allowed to quench with an aqueous solution of HCl (20 mL, 6.0 M). After removing the undesired solid from the reaction mixture by simple filtration, the filtrate was dried over anhydrous Na₂SO₄ and concentrated under reduced pressure to afford desired prenylamine hydrochloride. Aq. NaOH (10 mL, 6.0 M) was allowed to pour into the amine salt, and extraction of the resultant solution was performed with Et₂O (3×50 mL). The combined organic layer was allowed to dry over anhydrous Na₂SO₄ and the solvent was eliminated in vacuum to afford the desired amine 1c (1.37 g, 54 %).⁵

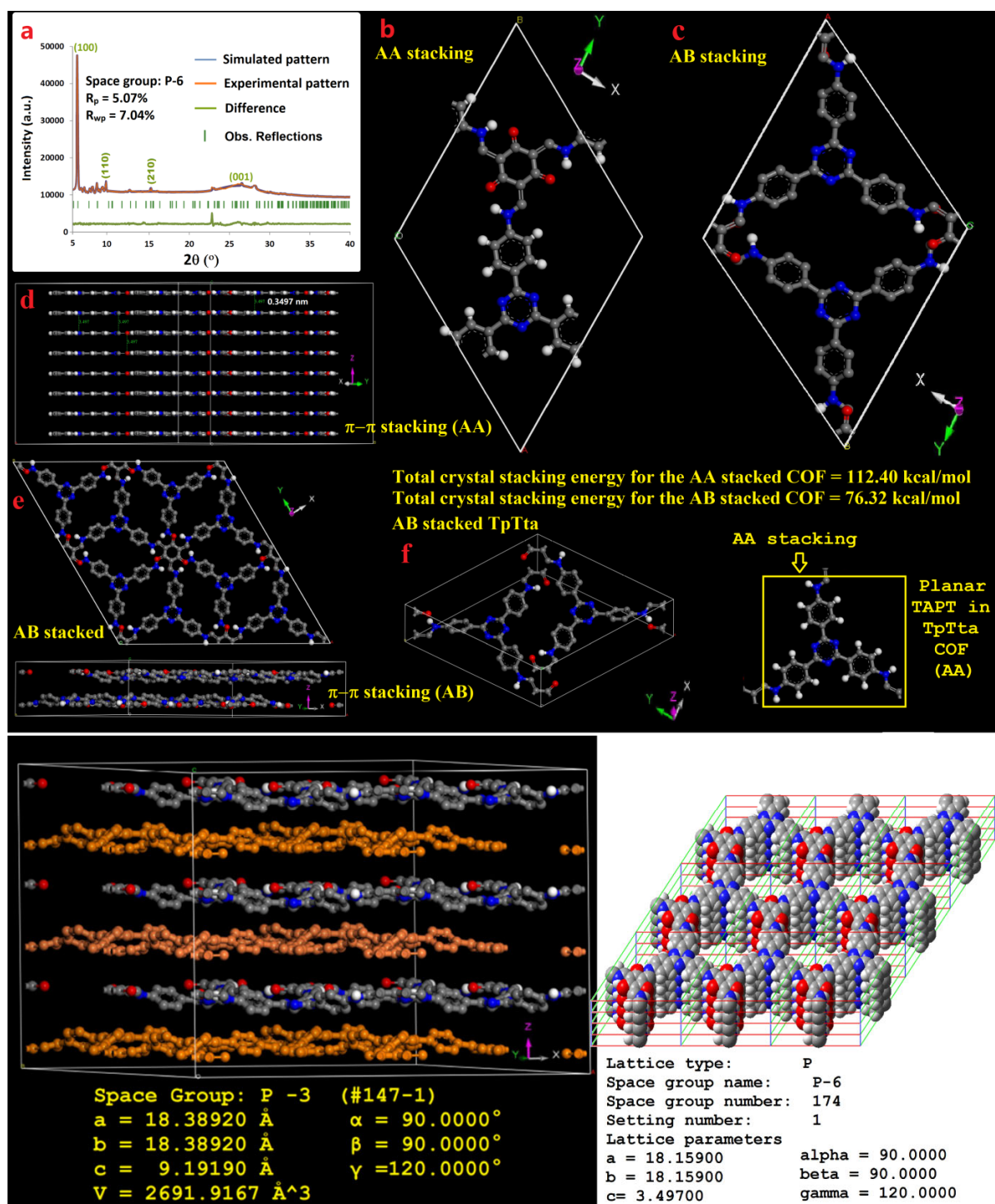


Figure S8. Theoretical evaluation and experimental PXRD of TpTta (a), packing arrangement for simulated AA stacking (b), packing arrangement for simulated AB stacking (c, e, f), π - π stacking showing interlayer spacing of about 0.3497 nm for eclipsed structure (AA), in which triazine units are planar and higher calculated total crystal stacking energy in contrast to AB staggered structure, revealing AA eclipsed arrangement (d).

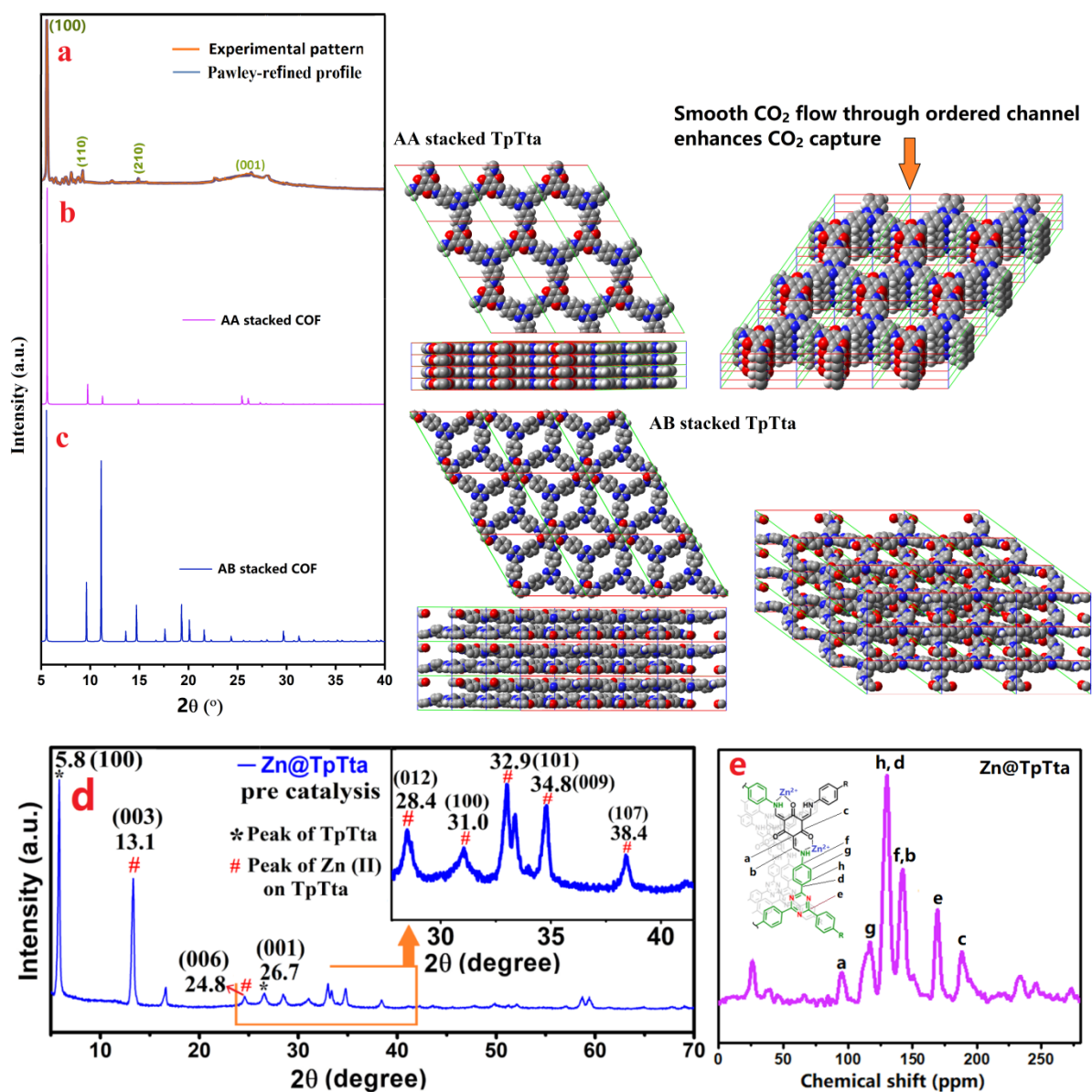


Figure S9. The experimental profile in orange and Pawley-refined profile in blue (a), PXRD patterns and view of the AA stacking arrangement (b), AB stacking crystal arrangement (c) of TpTta, and PXRD pattern of Zn@TpTta material (d), ¹³C solid-state CP/MAS NMR spectrum of the Zn(II) embedded COF catalyst (e).

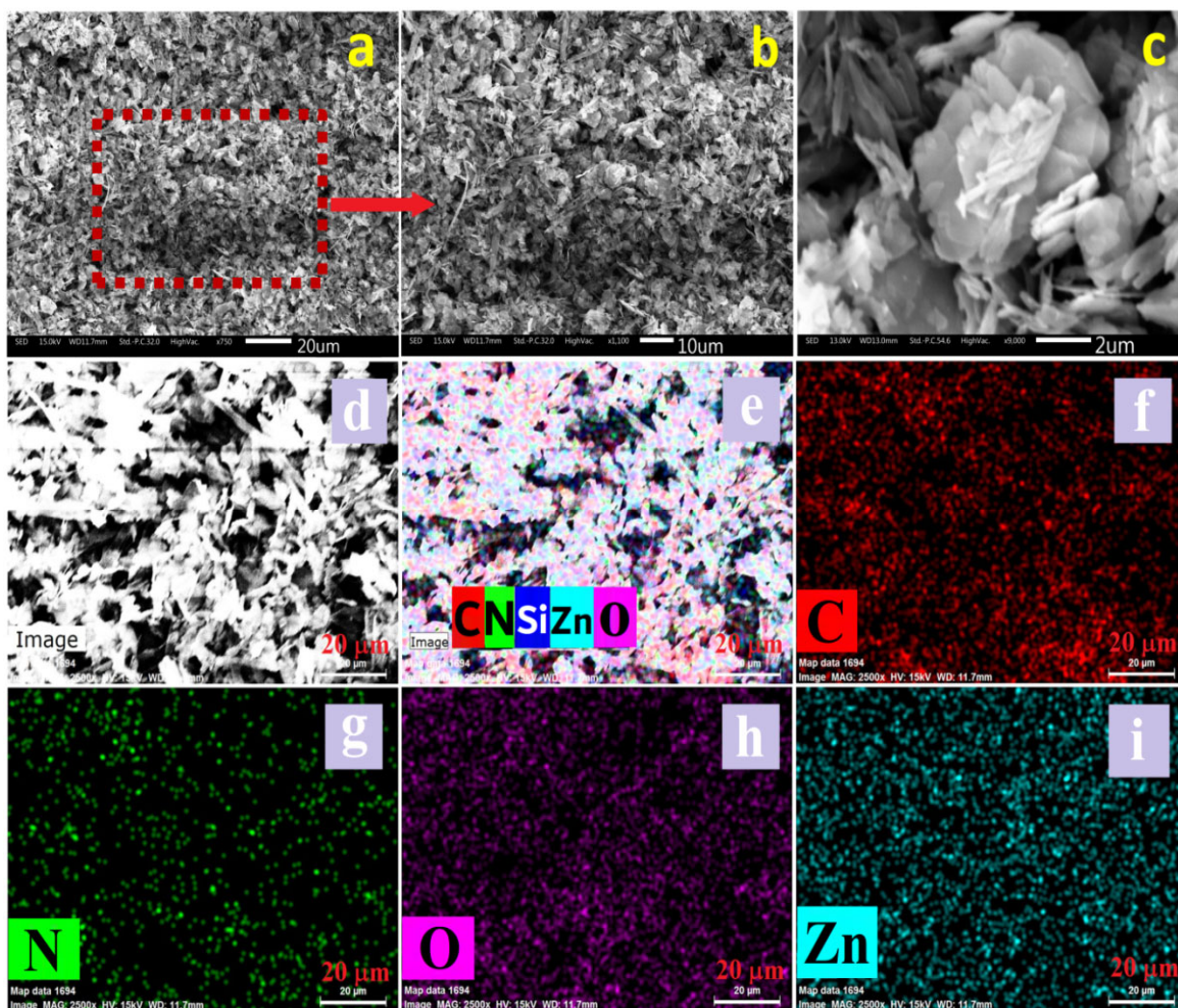


Figure S10. FE-SEM pictures of Zn@TpTta catalyst at several magnifications (a-c). Energy dispersive spectroscopy (EDS) elemental mapping images of the Zn(II)-loaded COF. Elemental mapping (C (red), N (green), O (magenta), Zn (Seafoam Green) pictures of the Zn-based COF catalyst.

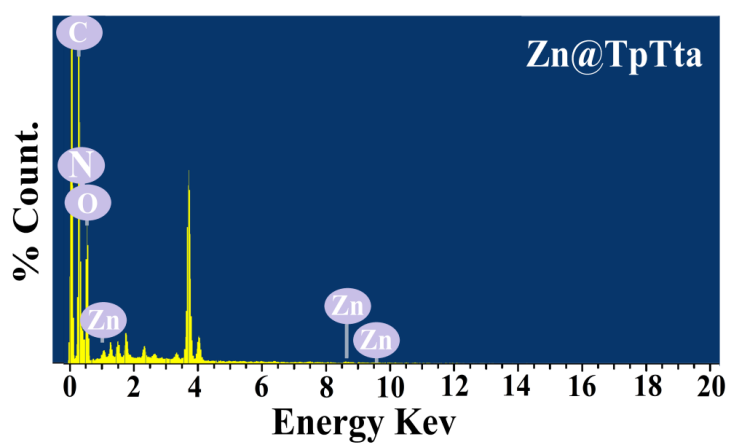


Figure S11. EDAX pattern of Zn@TpTta.

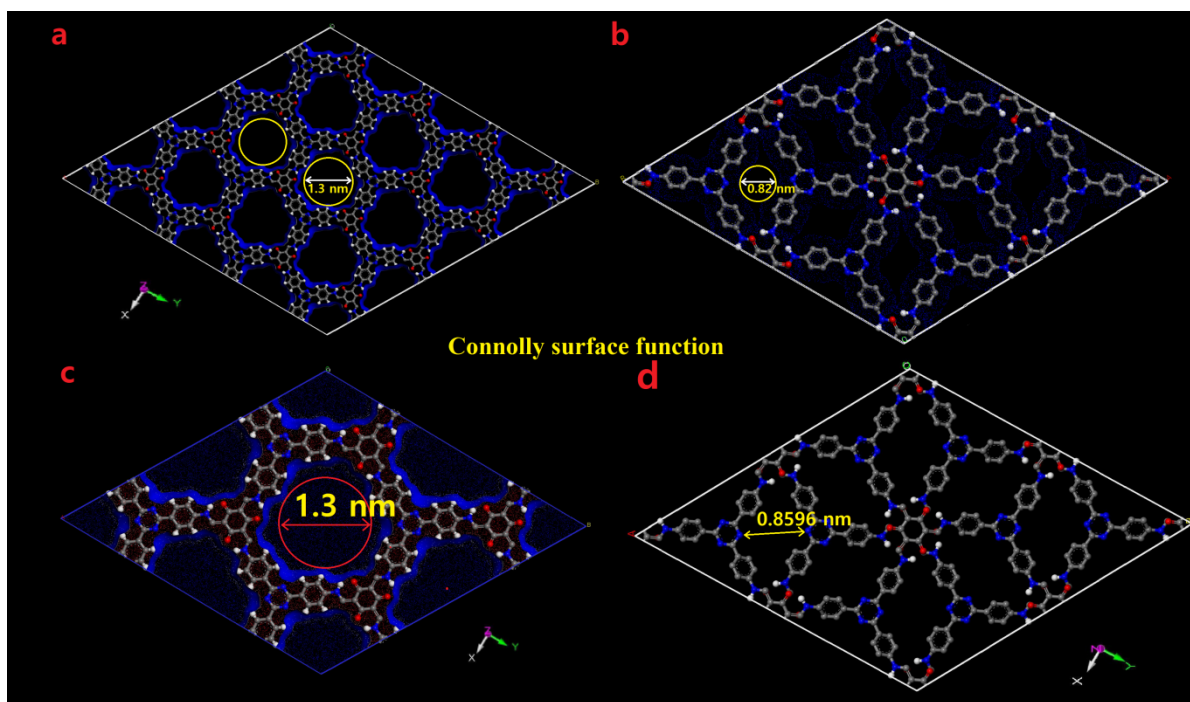


Figure S12. Connolly surface function of the synthesized 2D COF. Model structures employed for prediction of pore diameter (a,c) AA-eclipsed structure and (b,d) AB-staggered structure.

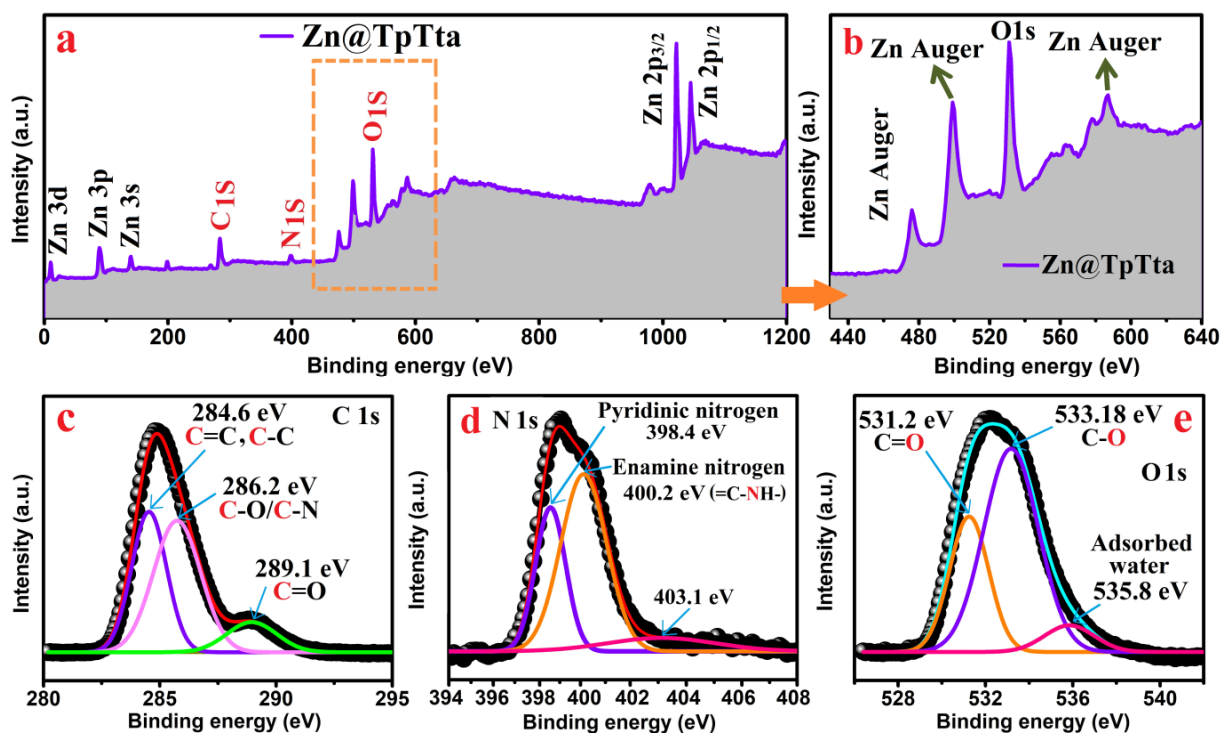


Figure S13. Overall XPS survey scan measurement on the laboratory-fabricated metal-based catalyst (Zn@TpTta) (a), zoom-in spectrum of Zn@TpTta showing Zn Auger (b), narrow scan C 1s (c), narrow scan N 1s (d) and narrow scan O 1s measurement (e) on the laboratory-fabricated metal-based catalyst (Zn@TpTta).

The UV-Vis experiment of the Zn(II)-anchored triazine-based COF named as Zn@TpTta is revealed in Fig. S14. Two obvious absorption bands are observed from UV-vis spectrum. The result obtained reveals that $\sigma \rightarrow \sigma^*$ and $\pi \rightarrow \pi^*$ transitions are present, which may be caused by the existence of covalently bonded π -conjugated system in the fabricated material (Zn@TpTta). UV-Vis observation is used to gather hidden information on the interaction (a certain degree of chemical interaction) including coordination between Zinc ion and the as-synthesized COF. The values of binding constant K_a were normally in between 10^5 - 10^7 M^{-1} with little outliers. This demonstrates that the tendency of the ligand to bind to the metal ion (Zn(II)) is sufficient to form a stable complex in this coupling reaction. A clearly visible peak positioned at around 260 nm is related to the strong interaction between Zn(II) and covalently bonded π -conjugated COF featuring several enamine units.⁷⁹

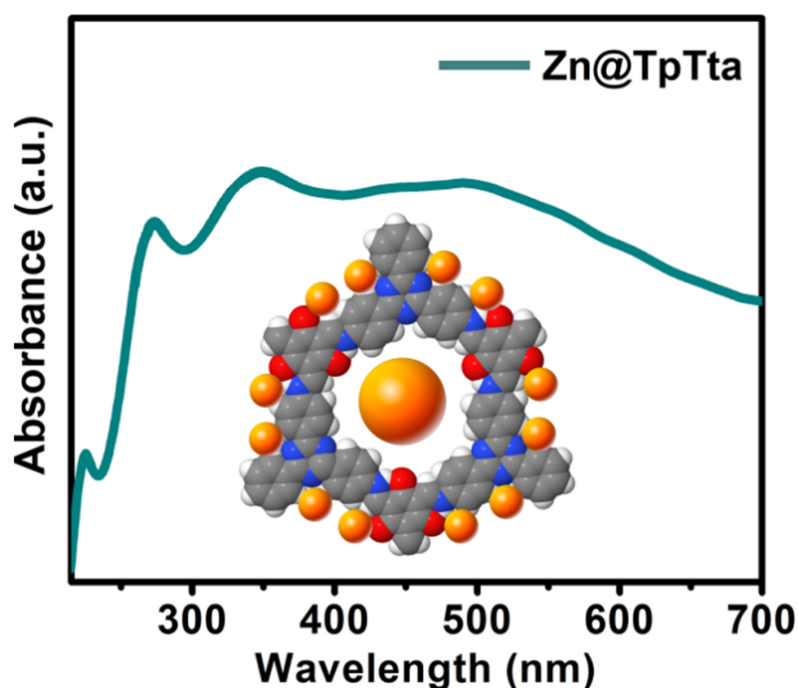


Figure S14. UV-Vis absorption spectrum of Zn(II)-anchored triazine-based COF (Zn@TpTta).

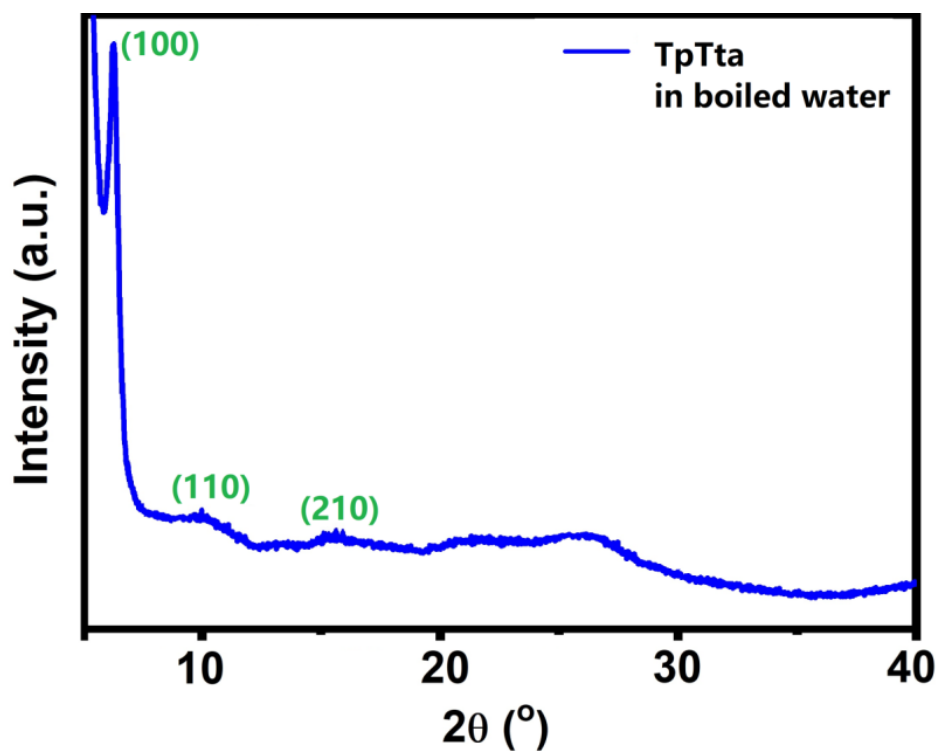


Figure S15. PXRD pattern of the as-obtained COF (TpTta) after treatment with boiled water.

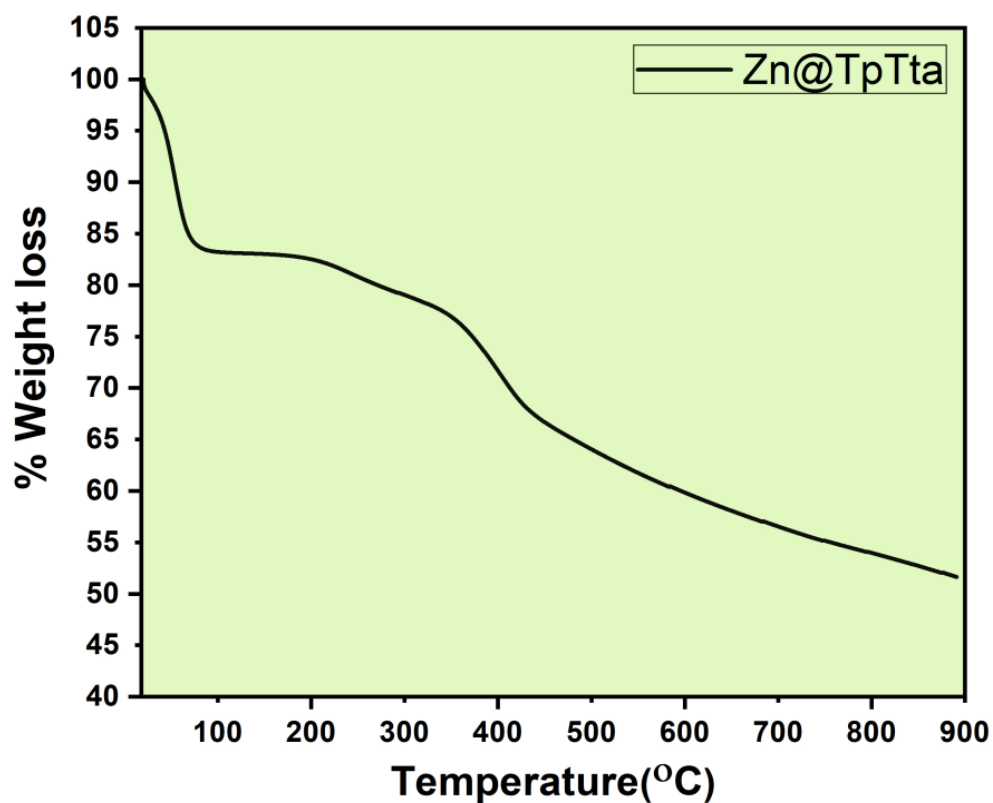


Figure S16. Thermogravimetric analysis (TGA) of the formed Zn@TpTta catalyst.

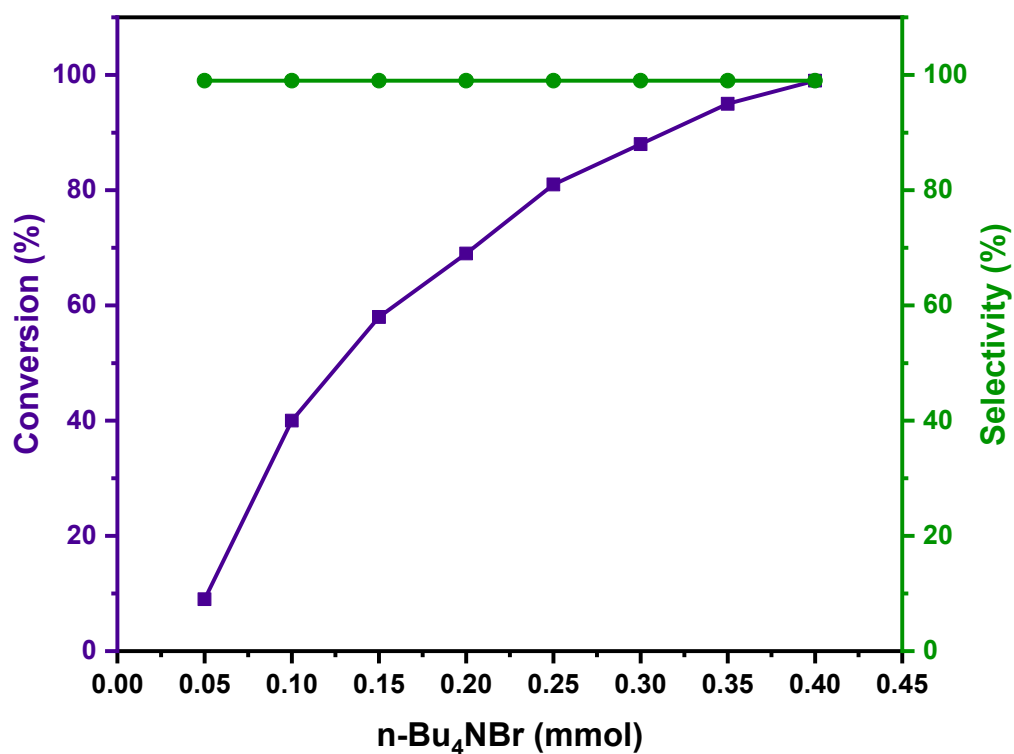


Figure S17. Impact of n-Bu₄NBr amount in CO₂ and cycloaddition reaction of ECH [Zn@TpTta: 30 mg, 1 atm CO₂, 60 °C, 10 h]

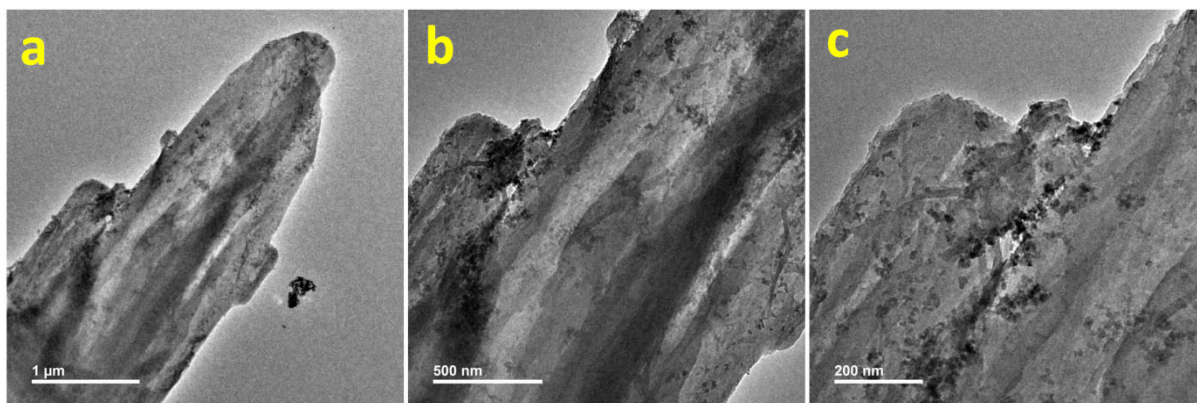


Figure S18. The UHR-TEM pictures of the recovered Zn@COF sheets at various scales (a) 1 μm, (b) 500 nm, and (c) 200 nm after 5th run.

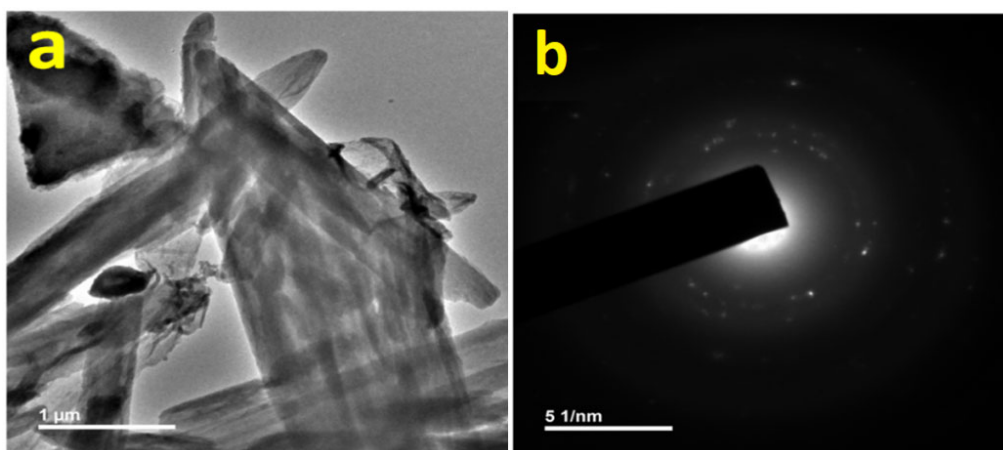
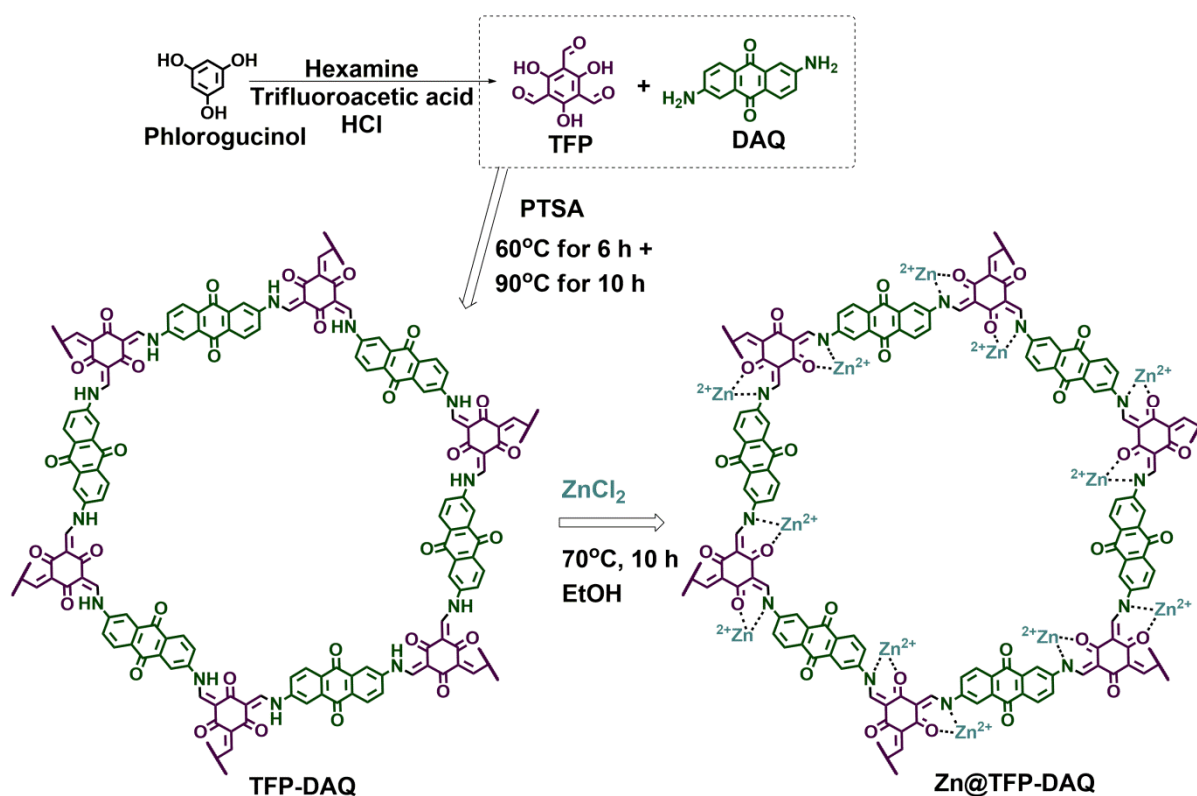


Figure S19. The UHR-TEM pictures of the COF sheets in boiled water (a) and SAED pattern of the COF (boiled water) (b).



Scheme S1. Schematic representation of the synthesis of Zn@TFP-DAQ

Synthesis of TFP- DAQ:

For the synthesis of TFP- DAQ, 7.5 mmol of *p*-toluenesulfonic acid (PTSA) was taken in a dry and clean mortar-pestle followed by the addition of 1.34 mmol 2,6-Diaminoanthraquinone (DAQ). The mixture was uniformly grinded for about 10 minutes. In this resulting mixture 0.9 mmol of TFP was carefully added followed by further grinding for about 15 minutes. To make the mixture viscous, few drops of distilled water were added. The resultant mixture was carefully transferred into an autoclave. The autoclave along with its

content was placed in an oven at 60°C for 6h followed by 90°C for another 10h. After cooling to room temperature, the resultant TFP-DAQ was washed for several times using *N,N*-dimethylacetamide and then with copious amount of acetone to remove impurities. Finally, it was allowed to dry under vacuum for 12h at room temperature to obtain the as-synthesized TFP-DAQ.

Synthesis of Zn@TFP-DAQ:

At first, as-prepared TFP-DAQ (1g) and anhydrous ZnCl₂ (0.1g) were taken in a RB flask containing ethanol (25ml). Then the RB flask along with its content was allowed to reflux at 70°C for 10h. After cooling to room temperature, the Zn grafted COF, Zn@TFP-DAQ was obtained through filtration and washed several times with excess amount of ethanol to remove any unreacted ZnCl₂. The material was dried under the application of vacuum condition at room temperature for 12h.

Powder X-ray diffraction (PXRD) analysis.

PXRD analysis was used to ascertain the ordered structure/crystallinity of the TFP-DAQ and Zn@TFP-DAQ. The PXRD patterns of the as-synthesized COF and Zn-based COF exhibit a diffraction peak of high intensity at a diffraction angle (2θ) of 3.5, which arises from 100 facet demonstrating hexagonal structure of the synthesized material. The hump-shape peak situated at a diffraction angle of 26.9 for TFP-DAQ and 27.0 for Zn@TFP-DAQ are due to π - π stacking among the aromatic ring, revealing the presence of layer-by-layer COF structure.

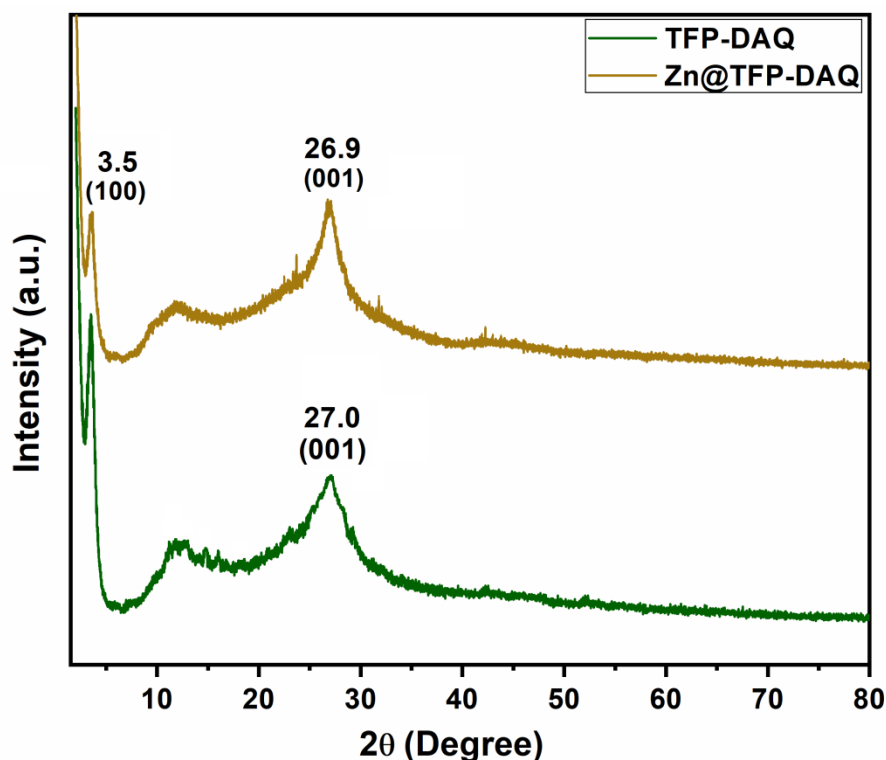


Figure S20. PXRD pattern of Zn@TFP-DAQ.

BET Surface area measurement:

N₂ sorption isotherm was performed at 77K to examine permanent porosities and to obtain BET surface area of the as-synthesized Zn@TFP-DAQ. The sorption curve of Zn@TFP-DAQ displays type I pattern with additional features of type IV pattern, which confirms the existence of micropores and mesopores in the synthesized material. The observed BET surface area of the as-synthesized Zn@TFP-DAQ was 789.375 m²g⁻¹.

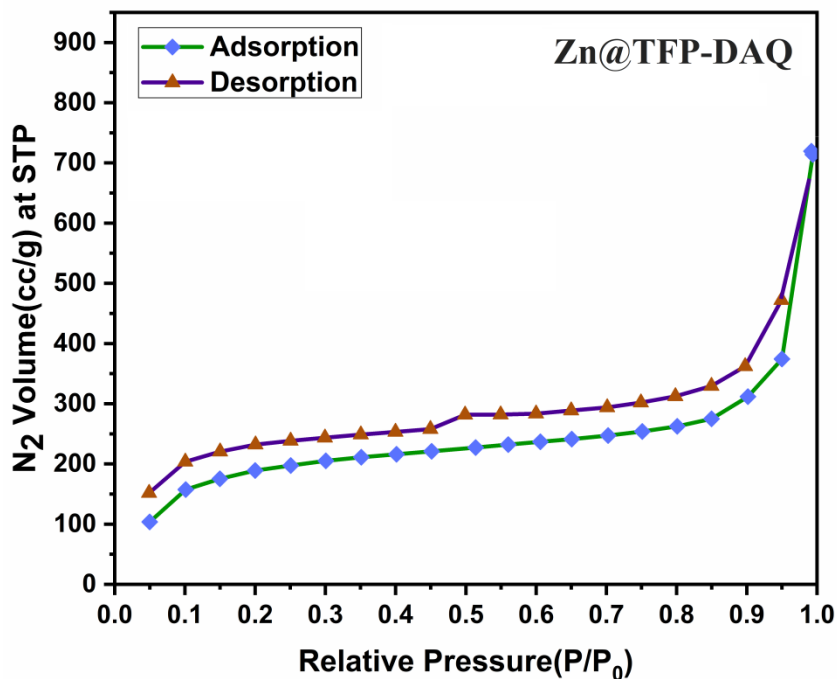
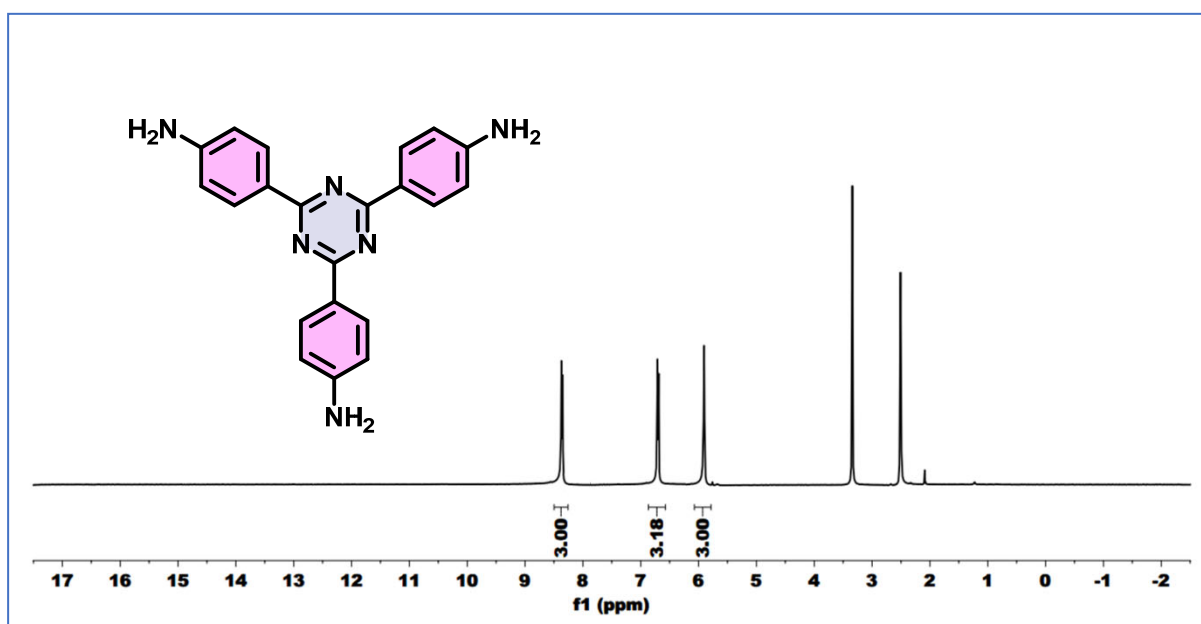
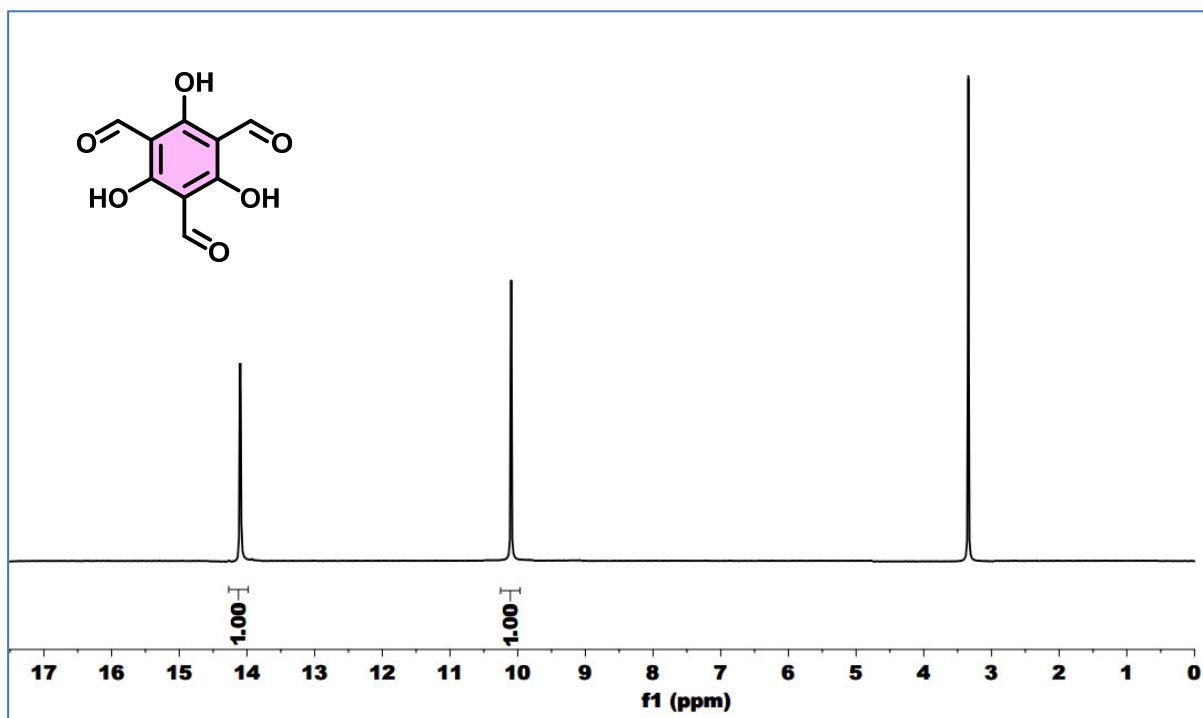


Figure 21. N₂ gas sorption isotherm of Zn(II)-functionalized COF (Zn@TFP-DAQ).

¹H NMR spectrum of 1,3,5-tris-(4-aminophenyl)triazine (TAPT)

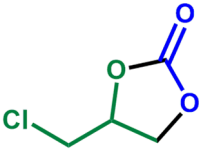


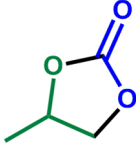
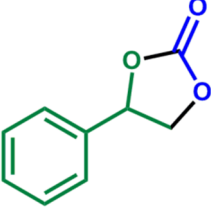
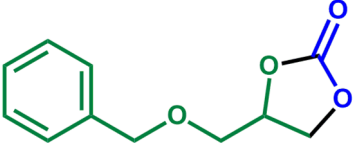
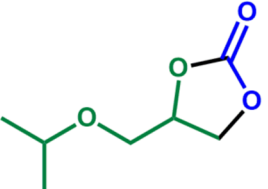
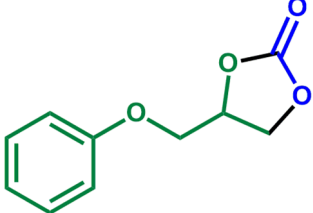
^1H NMR spectrum of 2,4,6-trihydroxybenzene-1,3,5-tricarbaldehyde



NMR Spectra of Cyclic Carbonates

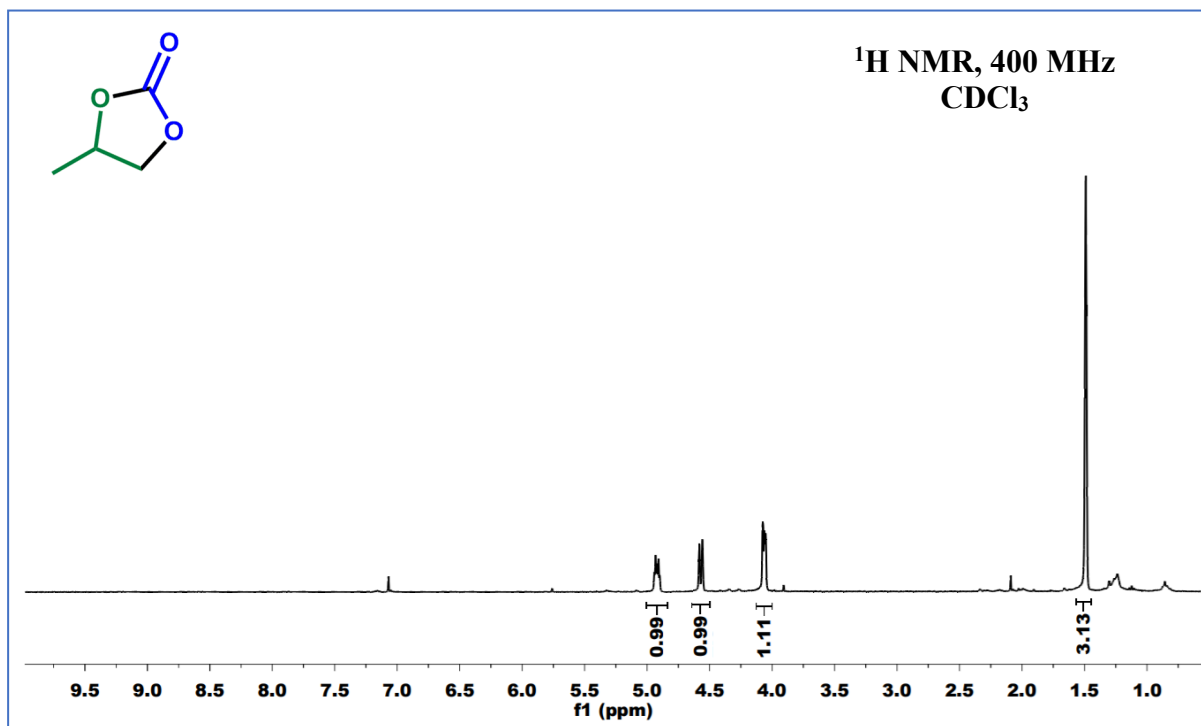
^1H NMR data of isolated pure cyclic carbonate derivatives:

 2a	^1H NMR (400 MHz, CDCl_3): δ 3.69-3.83 (m, 2H), 4.40-4.44(m, 1H), 4.58-4.62(t, $J=8\text{Hz}$, 1H), 4.96-5.02(m, 1H)
2b	^1H NMR (400 MHz, CDCl_3): δ 2.77 (br s, 1H), 3.64-3.70 (m, 1H), 3.91-3.96(m, 1H), 4.38-4.48(m, 2H), 4.78(m, 1H)
2c	^1H NMR (400 MHz, CDCl_3): δ 3.61-3.66(m, 1H), 3.68-3.73(m, 1H), 4.03-4.09(m, 2H), 4.39-4.43(m, 1H), 4.50-4.54(m, 1H), 4.82-4.87(m, 1H), 5.23-5.31(m, 2H), 5.83-5.93(m, 1H)

 <p style="text-align: center;">2d</p>	$^1\text{H NMR (400 MHz, CDCl}_3\text{): } \delta$ 1.48-1.50(d, J=8.0Hz, 3H), 4.03-4.07(m,1H), 4.56-4.60(t, J=8Hz, 1H), 4.86-4.92(m,1H)
 <p style="text-align: center;">2e</p>	$^1\text{H NMR (400 MHz, CDCl}_3\text{): } \delta$ 4.12-4.16 (m, 1H), 4.58-4.63 (m, 1H), 5.50-5.54 (t, J=8 Hz, 1H), 7.20-7.31(m, 5H)
<p style="text-align: center;">2f</p>	$^1\text{H NMR (400 MHz, CDCl}_3\text{): } \delta$ 1.31-1.41 (m, 2H), 1.50-1.59 (m, 2H), 2.06-2.14 (m, 4H), 4.57-4.66 (m, 2H) ppm.
 <p style="text-align: center;">2g</p>	$^1\text{H NMR (400 MHz, CDCl}_3\text{): } \delta$ 2.58-2.60(m, 1H), 2.76-2.78(m, 1H), 3.15-3.18(m, 1H), 3.38-3.43(dd, J=11.8, 6Hz, 1H), 3.73-3.76(dd, J=11.8, 2.8Hz, 1H), 4.52-4.61(m, 2H), 7.26-7.34(m, 5H)
 <p style="text-align: center;">2h</p>	$^1\text{H NMR (400 MHz, CDCl}_3\text{): } \delta$ 1.15-1.17(d, J=8Hz, 6H), 3.53-3.69 (m, 3H), 4.37-4.40 (m, 1H), 4.48-4.52(m, 1H), 4.80-4.83(m, 1H)
 <p style="text-align: center;">2i</p>	$^1\text{H NMR (400 MHz, CDCl}_3\text{): } \delta$ 4.06-4.19(m,2H), 4.51-4.63 (m, 2H), 5.01-5.03(m,1H), 6.90-7.03(m,3H), 7.26-7.33(m,2H)

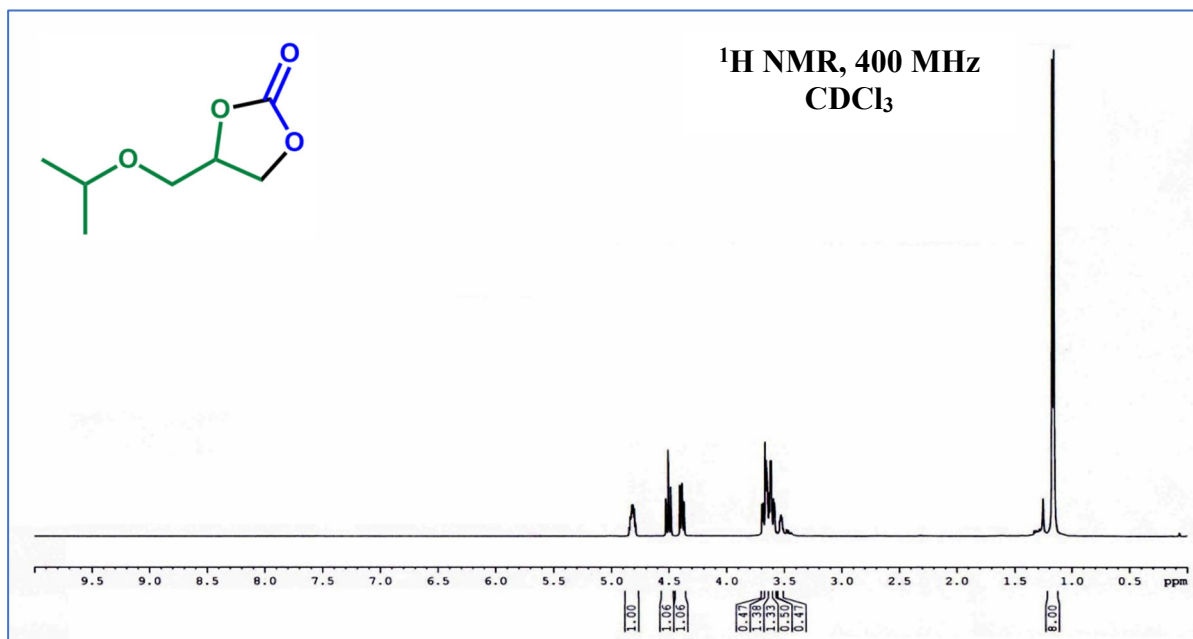
4-methyl-1,3-dioxolan-2-one

¹H NMR spectra:



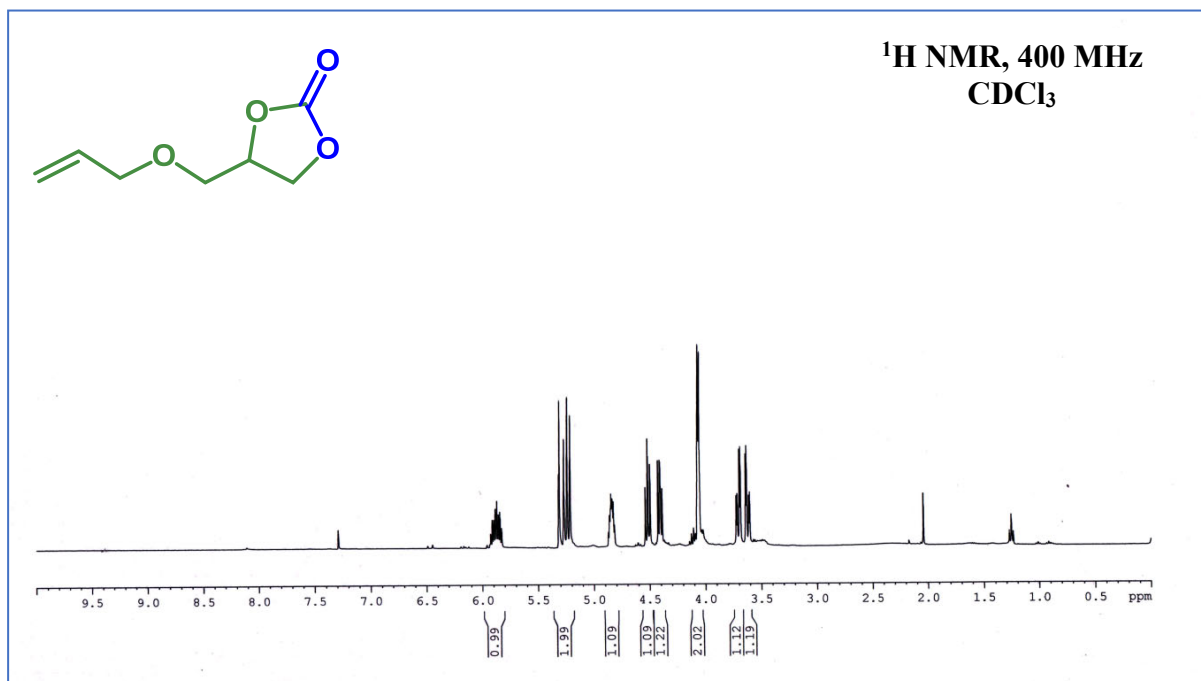
4-(isopropoxymethyl)-1,3-dioxolan-2-one

¹H NMR spectra:



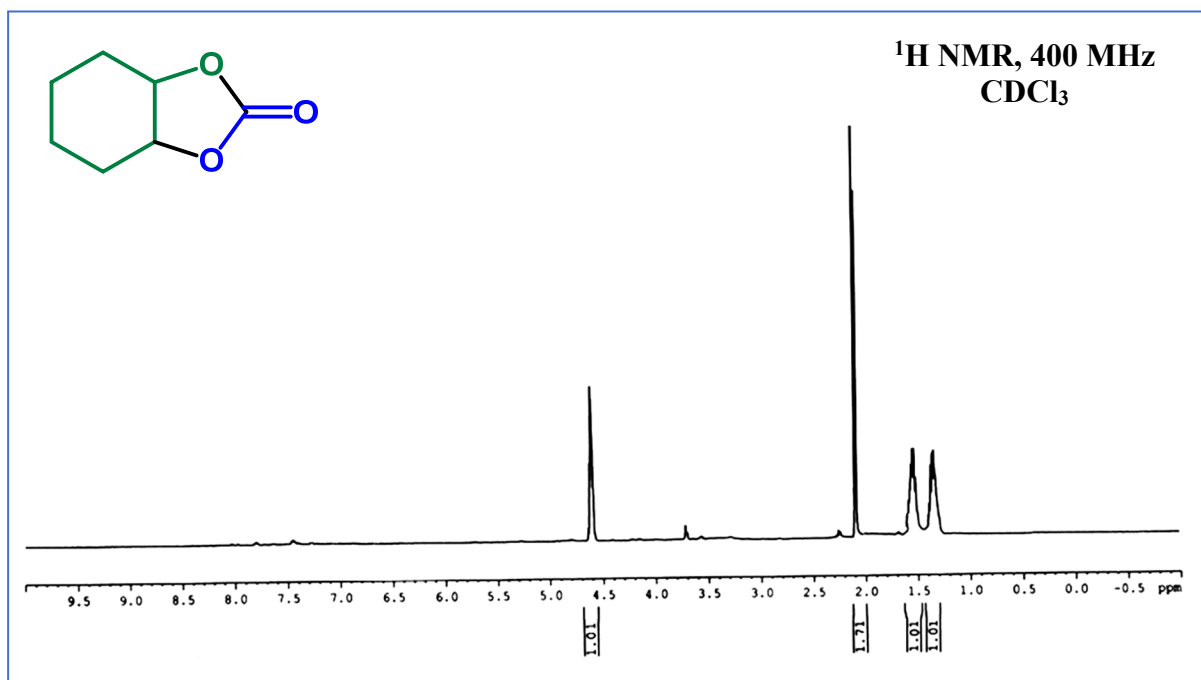
2-(allyloxymethyl)oxirane

^1H NMR spectra:



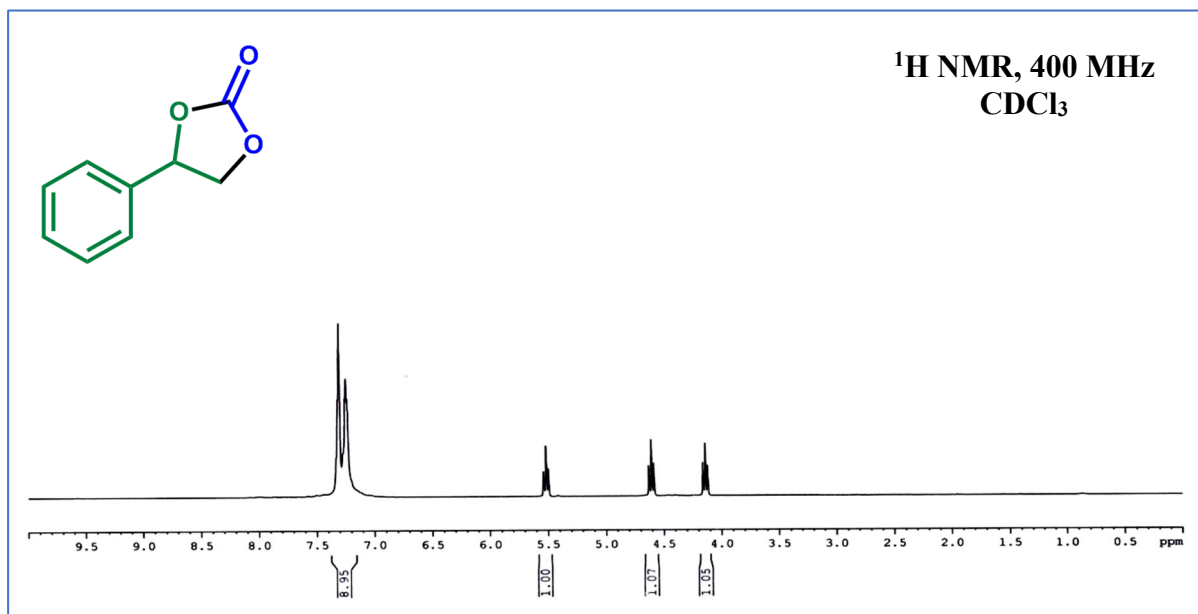
Hexahydro-benzo[1,3]dioxol-2-one

^1H NMR spectra:



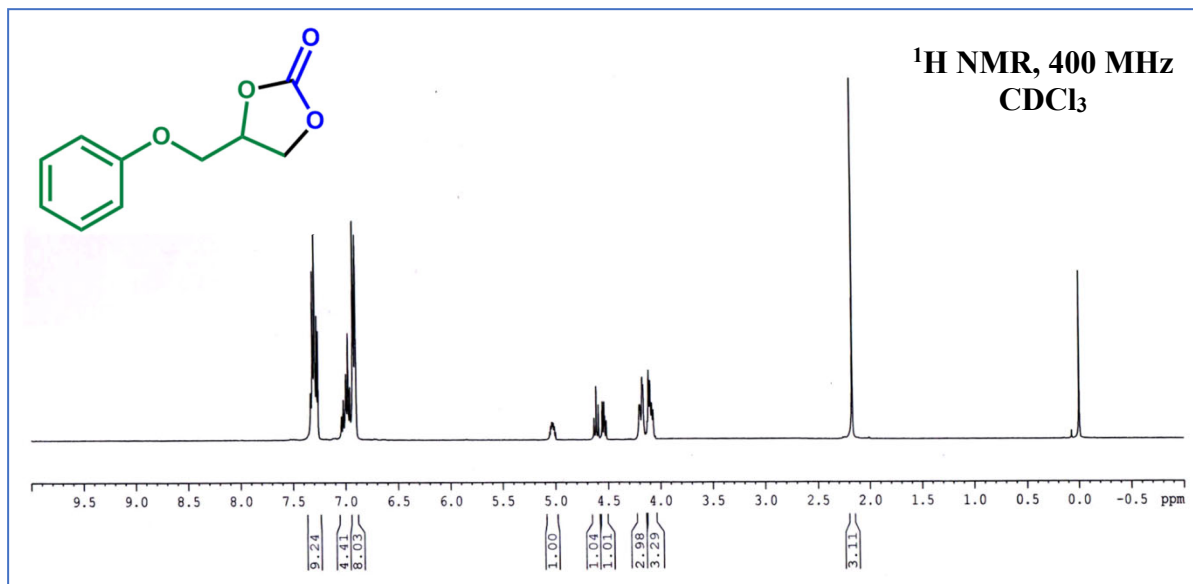
4-phenyl-1,3-dioxolan-2-one

¹H NMR spectra:



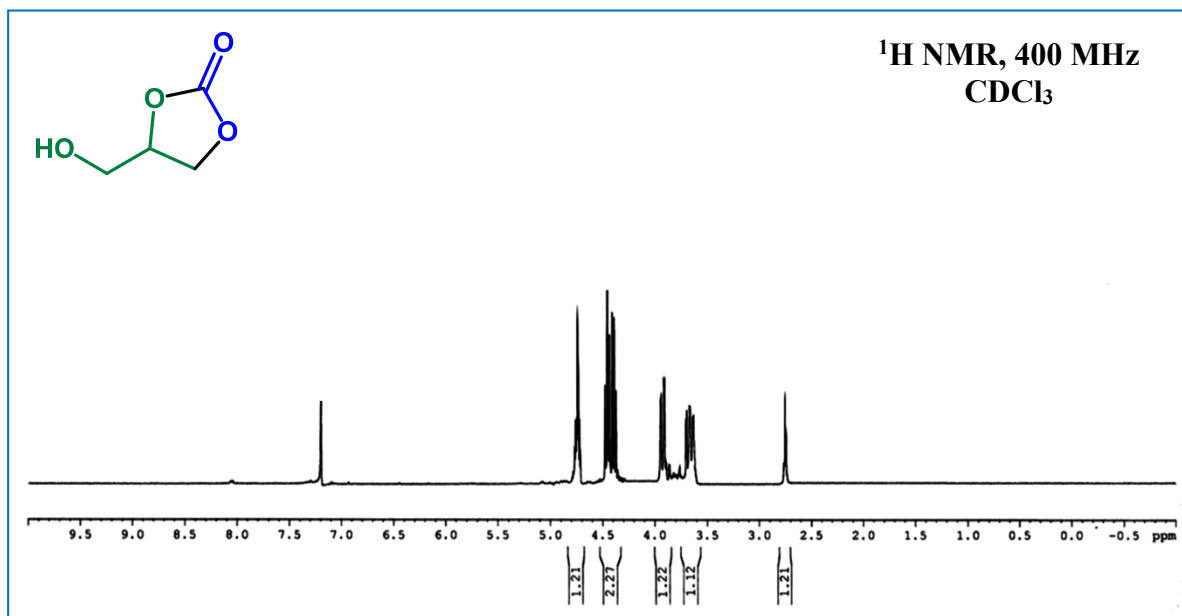
4-(phenoxyethyl)-1,3-dioxolan-2-one

¹H NMR spectra:



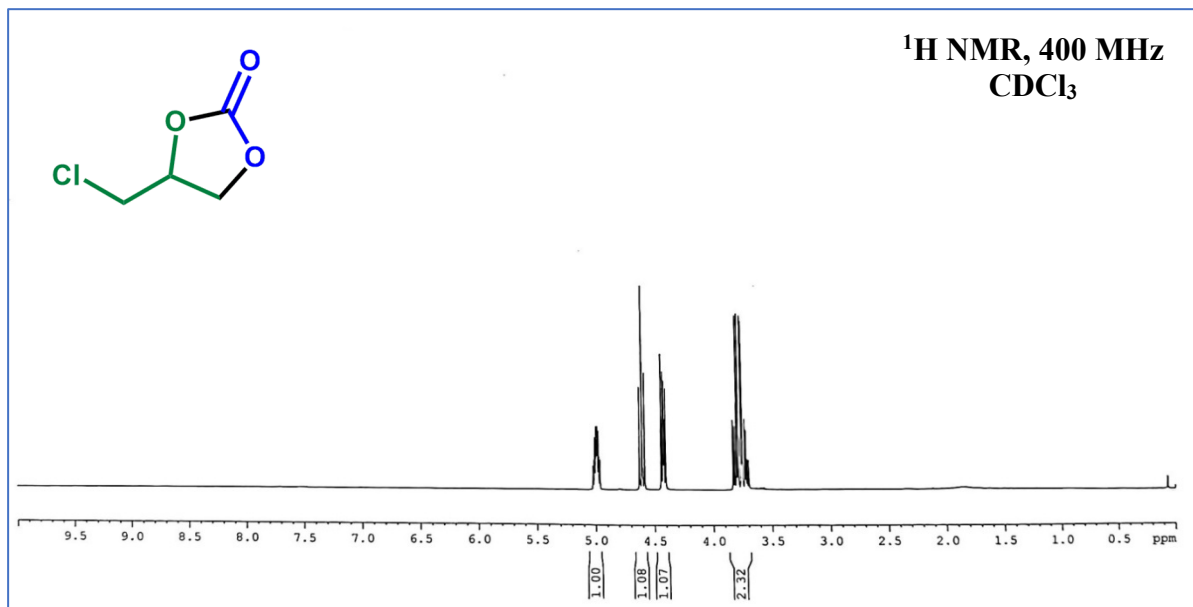
4-(Hydroxymethyl)-1,3-dioxolan-2-one

¹H NMR spectra:



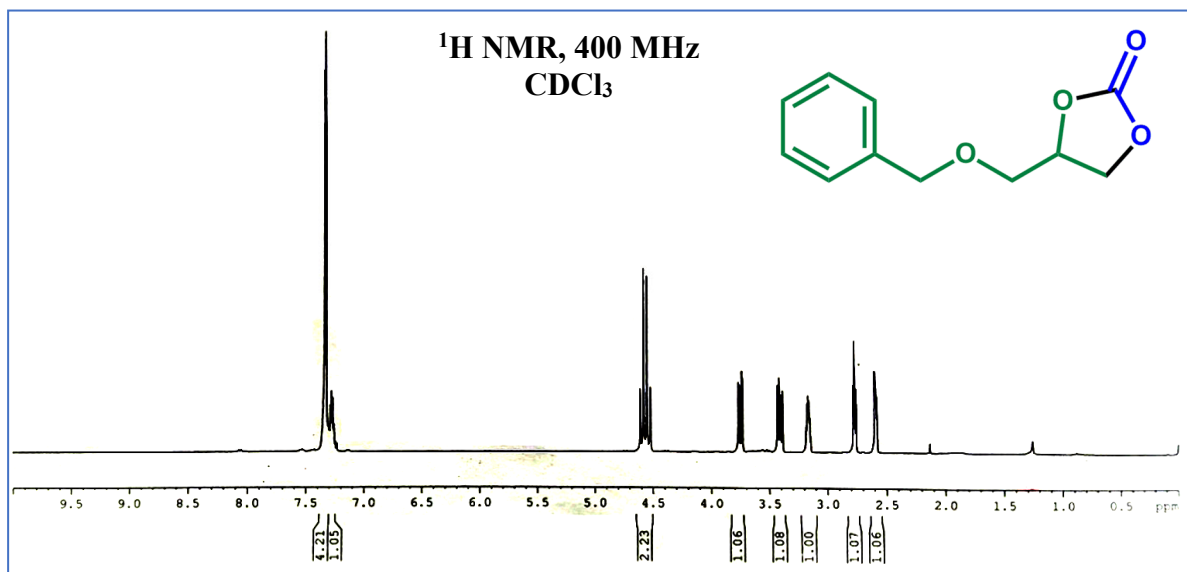
4-(chloromethyl)-1,3-dioxolan-2-one

¹H NMR spectra:



4-((benzyloxy)methyl)-1,3-dioxolan-2-one

¹H NMR spectra:



NMR Spectra of Cyclic Carbamates

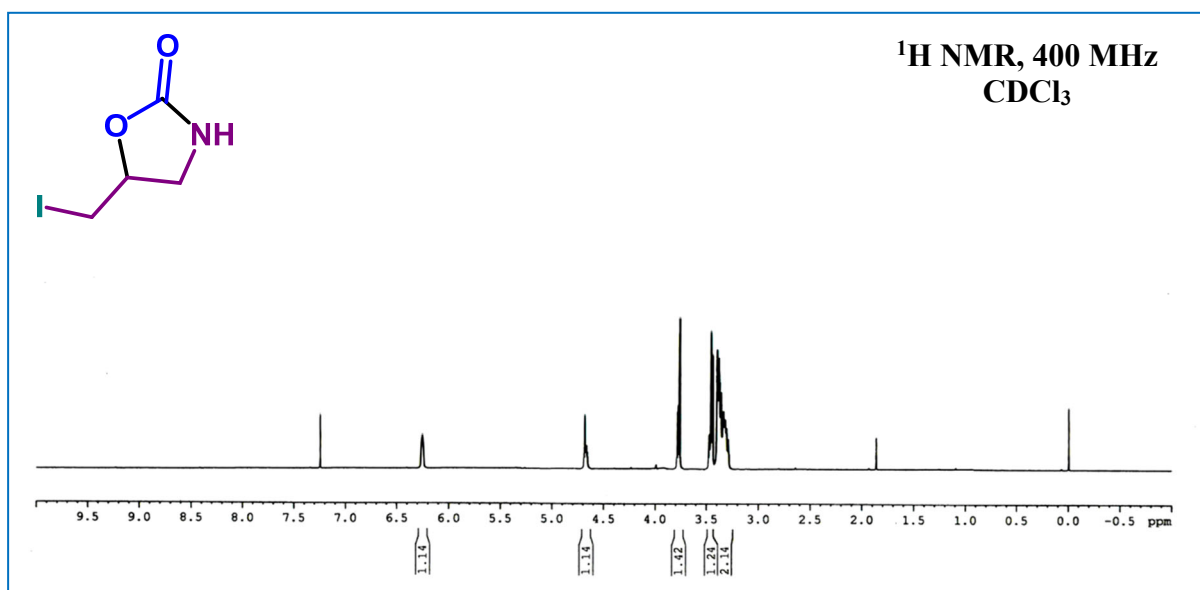
¹H NMR data of isolated pure cyclic carbamate derivatives:

4a	¹ H NMR (CDCl ₃): δ 3.28–3.48 (m, 3H), 3.78 (dd, 1H, <i>J</i> = 8.7, 8.7 Hz), 4.76 (m, 1H), 6.23 (br, s, 1H)
4b	¹ H NMR (CDCl ₃): δ 1.71 (s, 3H), 3.38 (d, 1H, <i>J</i> = 8.8 Hz), 3.42 (dd, 2H, <i>J</i> = 10.6, 17.1 Hz), 3.66 (d, 1H, <i>J</i> = 8.7 Hz), 5.99 (br, s, 1H)
4c	¹ H NMR (CDCl ₃): δ 1.59 (s, 3H), 1.58 (s, 3H), 3.74 (m, 2H), 4.21 (dd, 1H, <i>J</i> = 5.8, 8.3 Hz), 7.38 (br, s, 1H)

4d	¹ H NMR (CDCl ₃): δ 3.18–3.42 (m, 3H), 3.68 (t, 1H, <i>J</i> = 9.3 Hz), 3.88 (m, 2H), 4.58 (m, 1H), 5.26 (m, 2H), 5.71–5.86 (m, 1H)
4e	¹ H NMR (CDCl ₃): δ 1.92 (m, 1H), 2.28 (m, 1H), 3.28 (dd, 1H, <i>J</i> = 7.7, 10.6 Hz), 3.38–3.46 (m, 3H), 4.31 (m, 1H), 6.18 (br, s, 1H)
4f	¹ H NMR (CDCl ₃): δ 1.22–1.86 (m, 8H), 2.54 (td, 2H, <i>J</i> = 4.2, 13.1 Hz), 5.72 (s, 1H), 7.89 (br, s, 1H)

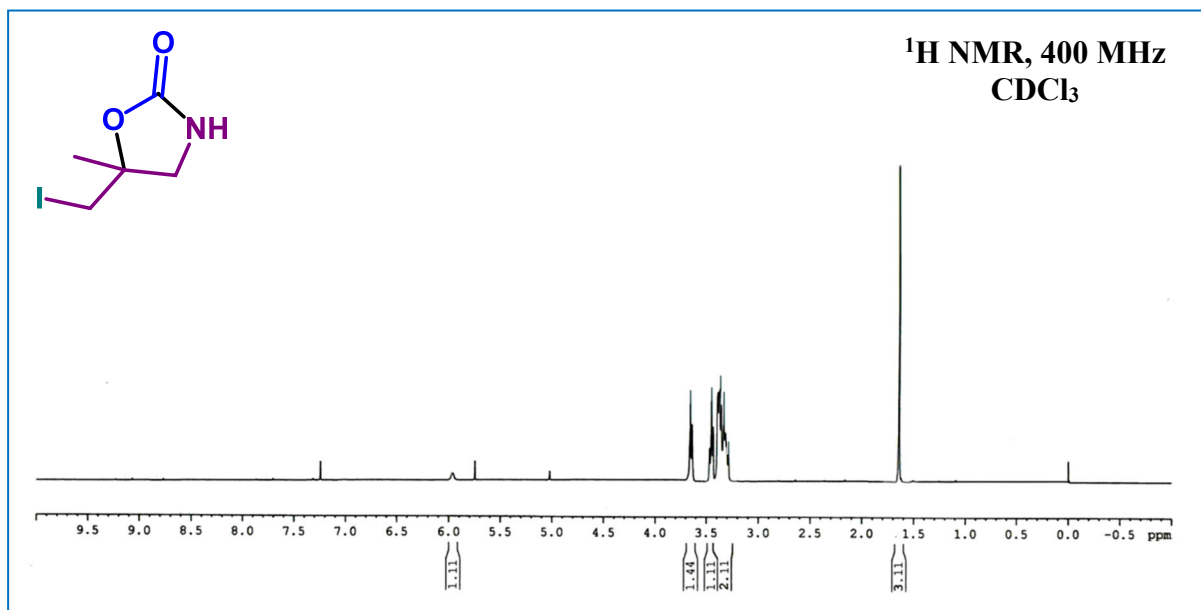
5-(Iodomethyl)-oxazolidin-2-one

¹H NMR spectra:



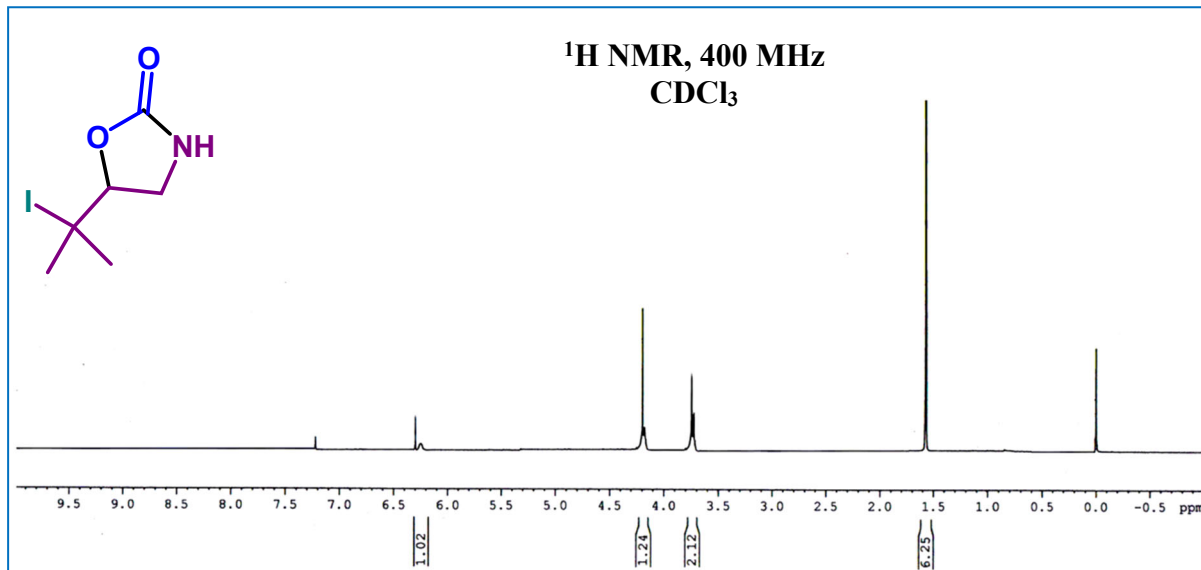
5-(Iodomethyl)-5-methyloxazolidin-2-one

¹H NMR spectra:



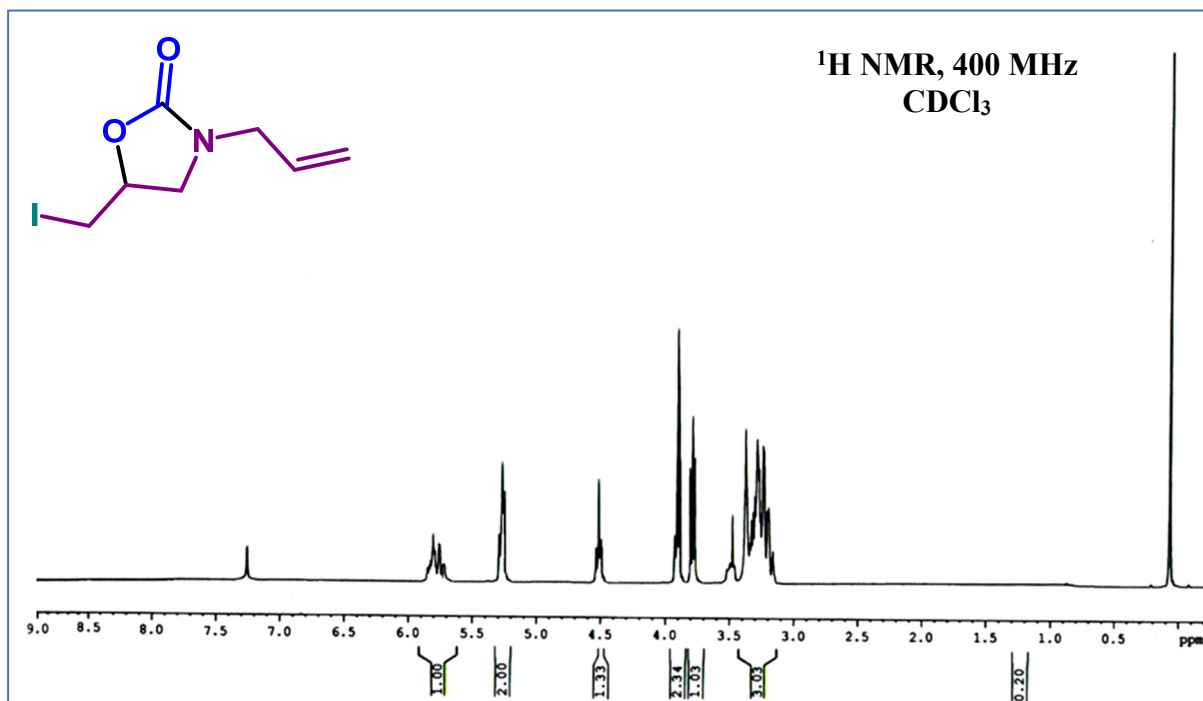
5-(2-Iodopropane-2-yl)oxazolidin-2-one

¹H NMR spectra:



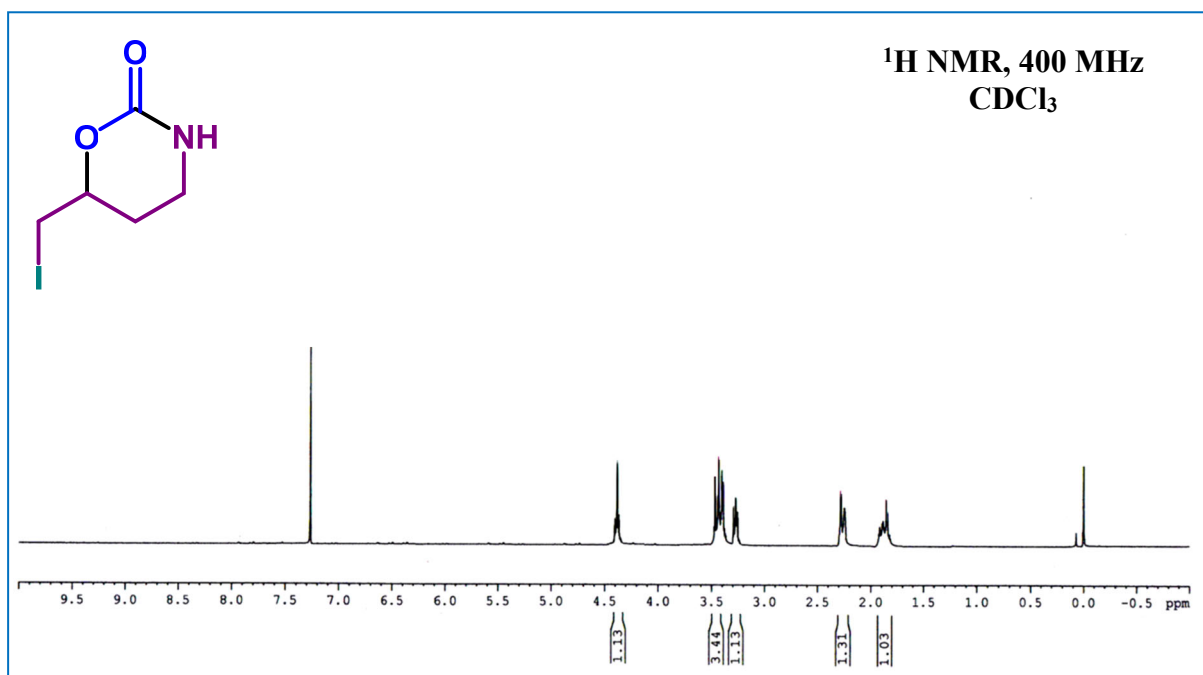
3-Allyl-5-(iodomethyl)oxazolidin-2-one

¹H NMR spectra:



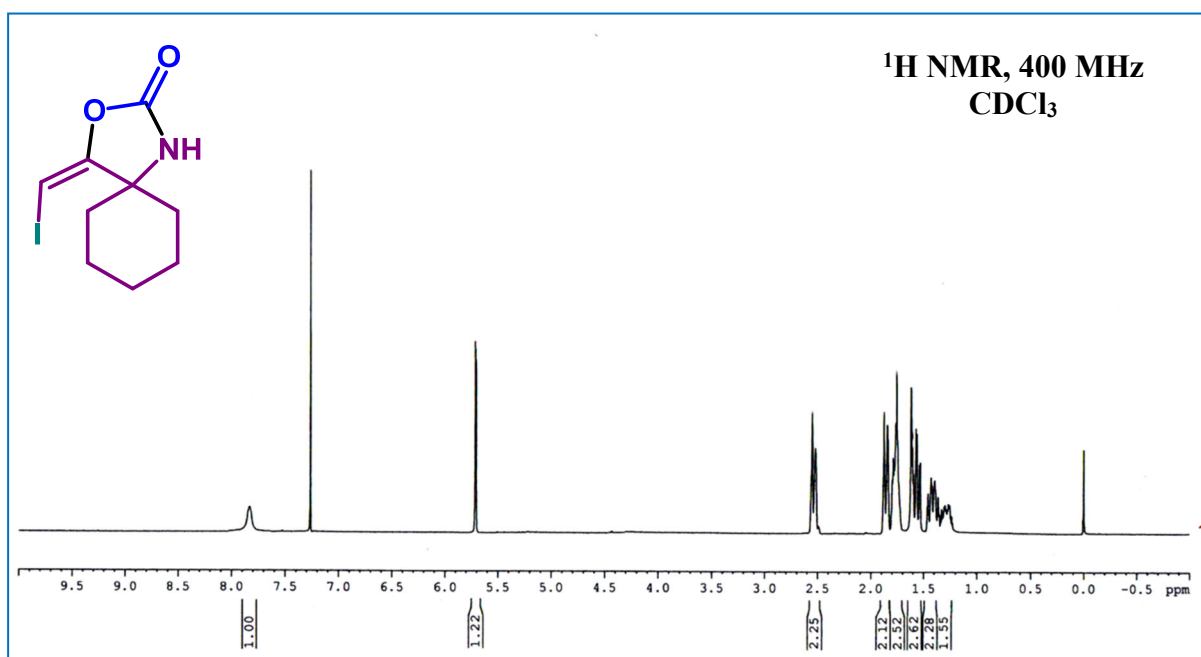
6-(Iodomethyl)-1,3-oxazinan-2-one

¹H NMR spectra:



(E)-4-(Iodomethylene)-3-oxa-1-azaspiro[4.5]decan-2-one

¹H NMR spectra:



References:

1. Jiang, C.; Jia, Q.; Tang, M.; Fan, K.; Chen, Y.; Sun, M.; Xu, S.; Wu, Y.; Zhang, C.; Ma, J.; Wang, C. Regulating the Solvation Sheath of Li Ions by Using Hydrogen Bonds for Highly Stable Lithium–Metal Anodes. *Angew. Chem. Int. Ed.* **2021**, *60*(19), 10871-10879.
2. Palafox, M. A.; Rastogi, V. K.; Vats, J. K. 4-Aminobenzonitrile: ab initio calculations, FTIR and Raman spectra. *Journal of Raman Spectroscopy: An International Journal for Original Work in all Aspects of Raman Spectroscopy, Including Higher Order Processes, and also Brillouin and Rayleigh Scattering*, **2006**, *37*(1-3), 85-99.
3. Karak, S.; Kandambeth, S.; Biswal, B. P.; Sasmal, H. S.; Kumar, S.; Pachfule, P.; Banerjee, R. Constructing ultraporous covalent organic frameworks in seconds via an organic terracotta process. *J. Am. Chem. Soc.* **2017**, *139*(5), 1856-1862.
4. Chong, J. H.; Sauer, M.; Patrick, B. O.; MacLachlan, M. J. Highly stable keto-enamine salicylideneanilines. *Org. Lett.* **2003**, *5*(21), 3823-3826.
5. Kukula, P.; and Koprivova, K. Structure-selectivity relationship in the chemoselective hydrogenation of unsaturated nitriles. *J. Catal.* **2005**, *234*(1), 161-171.